



*Aerospace Structures Information and Analysis Center*

## **Risk Analysis for Modeling Damage at Multiple Sites**

**Report No. TR-94-14**

**February 1994**

19990326 048

**Approved for public release; distribution is unlimited**

**DTIC QUALITY INSPECTED 4**

*Operated for the Flight Dynamics Directorate by CSA Engineering, Inc.*

REPORT DOCUMENTATION PAGE			Form Approved OMB No. 0704-0188	
Public reporting burden for this collection of information is estimated to average 1 hour per response, including the time for reviewing instructions, searching existing data sources, gathering and maintaining the data needed, and completing and reviewing the collection of information. Send comments regarding this burden estimate or any other aspect of this collection of information, including suggestions for reducing this burden, to Washington Headquarters Services, Directorate for Information Operations and Reports, 1215 Jefferson Davis Highway, Suite 1204, Arlington, VA 22202-4302, and to the Office of Management and Budget, Paperwork Reduction Project (0704-0188), Washington, DC 20503.				
1. AGENCY USE ONLY (Leave blank)		2. REPORT DATE February 1994		3. REPORT TYPE AND DATES COVERED Final Report 09/23/92 - 01/31/94
4. TITLE AND SUBTITLE Risk Analysis for Modeling Damage at Multiple Sites			5. FUNDING NUMBERS C-F33615-90-C-3211	
6. AUTHOR(S) Alan P. Berens, Joseph P. Gallagher, Subrato Dhar				
7. PERFORMING ORGANIZATION NAME(S) AND ADDRESS(ES) CSA Engineering, Inc. 2850 W. Bayshore Road Palo Alto, CA 94303			8. PERFORMING ORGANIZATION REPORT NUMBER  ASIAC-TR-94-14 UDR-TR-94-15	
9. SPONSORING/MONITORING AGENCY NAME(S) AND ADDRESS(ES) Flight Dynamics Directorate Wright Laboratory Air Force Materiel Command Wright-Patterson AFB, OH 45433-7562			10. SPONSORING/MONITORING AGENCY REPORT NUMBER	
11. SUPPLEMENTARY NOTES				
12a. DISTRIBUTION/AVAILABILITY STATEMENT  Approved for public release; distribution is unlimited.			12b. DISTRIBUTION CODE	
13. ABSTRACT (Maximum 200 words)  In this first phase of a two phase study to develop a computer program for risk analysis of fatigue damage at multiple sites, the computer code PROF was demonstrated to be applicable to the multi-element damage (MED) problem. The application requires the damage tolerant analysis and crack size input for each of the relevant structural elements and for the relevant combinations of intact and failed conditions of the subcritical structural elements on the critical elements. The demonstration was preformed incorporating the effects of two subcritical elements on the failure probability of the chordwise joint at WS405 of the C-141 airframe.  The application of PROF in the MSD area is not as clear. Since the largest crack in a lap joint will grow the fastest, the population of crack sizes to be modelled should be defined in terms of the largest crack in the zones of equivalent stresses. The sizes of the cracks in the holes immediately adjacent to the largest crack must be accounted for but several studies have indicated that the sizes of the cracks in more remote holes are not important drivers. Reasonable scenarios can be defined to bound the fracture probabilities given complete damage tolerant analyses and crack size data.				
14. SUBJECT TERMS Fracture, Damage Tolerance, Multi-Site-Damage (MSD), Risk Analysis			15. NUMBER OF PAGES 65	
			16. PRICE CODE	
17. SECURITY CLASSIFICATION OF REPORT Unclassified	18. SECURITY CLASSIFICATION OF THIS PAGE Unclassified	19. SECURITY CLASSIFICATION OF ABSTRACT Unclassified	20. LIMITATION OF ABSTRACT UL	

## FORWARD

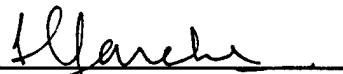
This report entitled "Risk Analysis For Modeling Damage at Multiple-Sites," documents a research program conducted at the University of Dayton Research Institute (UDRI) for the Aerospace Structures Information and Analysis Center (ASIAC) at Wright-Patterson AFB under subcontract to CSA Engineering, Inc. in support of the CSA Prime Contract No. F33615-90-C-3211, subcontract 91307.01, Task 40. The report presents the results of the first phase of a study whose ultimate objective is the application of risk analysis to multiple site damage. The effort was performed between September 1992 and December 1993.

The work documented herein was performed in the Structural Integrity Division of UDRI, under the general supervision of Mr. Blaine S. West, Division Head of the Aerospace Mechanics Division. Dr. Alan P. Berens was the Principal Investigator and significant technical contributions were made by Dr. Joseph P. Gallagher and Mr. Subrato Dhar. The CSA program manager was Jatin Parekh.

Approved by:



Gordon R. Negaard  
Principal Investigator



Jatin C. Parekh  
Program Manager

# *Table of Contents*

---

<u>Section</u>	<u>Page</u>
1 Introduction .....	1
2 Multi-Element Damage .....	3
2.1 Example Application of PROF to a Three-Element Structure .....	3
2.1.1 PROF Input Data for Example Three-Element Structure .....	5
2.1.2 Probabilities of Fracture for Example Three Element Structure .....	8
2.2 Discussion of PROF Multi-Element Analysis .....	10
3 Multi-Site Damage (MSD) .....	12
3.1 Geometric Parameters .....	13
3.2 Influence of Crack Size .....	15
3.3 Influence of the Longest Crack Size .....	16
3.3.1 Two Crack Configuration .....	16
3.3.2 Three Crack Configuration .....	18
3.4 Influence of Fracture Criteria and Material Properties .....	19
3.4.1 Fracture Criteria .....	19
3.4.2 Influence of Fracture Criteria .....	21
3.5 Discussion of MSD Results .....	22
4 Summary .....	24
5 References .....	25

## ***List of Tables***

---

<b><u>Table</u></b>		<b><u>Page</u></b>
1	List of PROF Input Data .....	6
2	Parameters for Distribution of Fracture Toughness .....	6
3	Weibull Crack Size Parameters .....	8
4	Geometric Parameters for Different Crack Configurations .....	14
5	A Summary of Critical Crack Location and Coalescence Strength .....	17
6	Material Properties. ....	21

## List of Figures

---

<b><u>Figure</u></b>		<b><u>Page</u></b>
1	Venn Diagram Partitioning the Event of Chordwise Joint Failure .....	28
2	$K/\sigma$ Versus Crack Length for WS405 Structural Elements .....	29
3	a Versus T - Chordwise Joint .....	30
4	a Versus T - Splice Fitting .....	31
5	a Versus T - Beam Cap .....	32
6	Distribution of Max Stress/Flight - Chordwise Joint .....	33
7	Distribution of Max Stress/Flight - Splice Fitting .....	34
8	Distribution of Max Stress/Flight - Beam Cap .....	35
9	Initial Crack Size Distributions at 31,000 Hours .....	36
10	POD for X-Ray Inspections - 'Have Cracks' Data .....	37
11	Conditional Failure Probabilities of Chordwise Joint - No Initial Inspection/Repair .....	38
12	Failure Probabilities of Splice Fitting and Beam Cap - No Initial Inspection/Repair .....	39
13	Unconditional Probability of Failure of Chordwise Joint - No Initial Inspection/Repair .....	40
14	Unconditional Probability of Failure of Chordwise Joint - With and Without Initial Inspection/Repair .....	41
15	Crack Configurations .....	42
16	Comparison of Residual Strength Levels between Infinite Collinear Cracks and Single Crack in an Infinite Sheet Based on Critical Stress Intensity Factor Criterion .....	43

## ***List of Figures (continue)***

---

<b><u>Figure</u></b>		<b><u>Page</u></b>
17	Comparison of Residual Strength Levels among (a) Single Crack, (b) Two Collinear Cracks, (c) Three Collinear Cracks and (d) Infinite Collinear Cracks, in an Infinite Sheet Based on Critical Stress Intensity Factor Criterion . . . . .	44
18	Ratio of Strength Levels for Extending Crack Tips B and A before Coalescence in Two Collinear Crack Configuration in an Infinite Sheet . . . . .	45
19	Ratio of Strength Levels for Extending Crack Tips B and D Before Coalescence in Two Collinear Crack Configuration in an Infinite Sheet . . . . .	46
20	Effect of the Largest Crack Size $a$ on Coalescence Strength at Crack Tip B in Two Collinear Crack Configuration in an Infinite Sheet . .	47
21	Effect of the Largest Crack Size $a$ on The Residual Strength Ratio (After/Before) in Two Collinear Crack Configuration in an Infinite Sheet .	48
22	Ratio of Strength Levels for Extending Crack Tips B and D Before Coalescence in Three Collinear Crack Configuration in an Infinite Sheet . . . . .	49
23	Effect of the Largest Crack Size $a$ on Residual Strength Ratio (After/Before) for Crack Tip D in Three Collinear Crack Configuration in an Infinite Sheet . . . . .	50
24	Swift Plastic Zone Interaction Model [22] . . . . .	51
25	K-R Curve [21] . . . . .	52
26	Effect of Fracture Criteria on the Residual Strength Level in an Infinite Collinear Cracks Configuration . . . . .	53
27	Effect of Fracture Toughness Level on Residual Strength Level in an Infinite Collinear Cracks Configuration . . . . .	54
28	Effect of Yield Strength Level on Residual Strength Level in an Infinite Collinear Cracks Configuration . . . . .	55

## ***List of Figures (concluded)***

---

<b><u>Figure</u></b>		<b><u>Page</u></b>
29	Comparison Between R-Curve and Stress Intensity Factor Criteria to Identify the Lower Bound for the Residual Strength Level in the Two Collinear Crack Configuration . . . . .	56
30	Comparison Between R-Curve and Swift Plastic Zone Criteria to Identify the Lower Bound for the Residual Strength Level in Two Collinear Crack Configuration . . . . .	57



# Section 1

## *Introduction*

---

The likelihood of damage at multiple sites in aging fleets of airframes has accentuated the need for evaluating the risks associated with fleet management decisions. Because of the existing damage tolerance analyses and data that result from the Air Force Aircraft Structural Integrity Programs, a fracture based risk analysis provides an immediate framework for calculating the increasing probabilities of catastrophic failure that are associated with the growing fatigue cracks of multiple site damage. For the conditions which degrade fail safety and damage tolerance capability, calculated risks of failure could form the basis for quantitative definitions of the onset of multiple site damage.

The computer program Probability Of Fracture (PROF) calculates single flight and interval failure probabilities for a single population of metallic details [1]. PROF uses the crack growth curves from the damage tolerance analysis of a detail to project an initiating crack size distribution in the expected usage environment. The probability of failure is calculated from the distributions of fracture toughness, maximum stress per flight, and the flight time dependent crack size distribution. Because multiple runs of PROF can be performed to model more complex structures and because PROF is structured around the generic damage tolerance analysis, this computer program can provide the basis for the risk analyses of multiple site damage scenarios.

A two phase effort was undertaken to implement the application of PROF to multiple site damage. The first phase comprised a study of potential multiple site damage scenarios to determine the nature of the changes that will be required to the PROF computer code. The second phase is the implementation of the necessary changes and the demonstration of the program. This report is an interim report which summarizes the activities of the first phase. It should be noted that all data continued herein are calculated data; no experimental study was performed in this effort.

Damage at multiple sites is considered to comprise both multi-element damage and

multi-site damage. Multi-element damage (MED) describes damage for which the stress intensity factors of the elements are not affected by crack sizes in the adjacent elements. The deleterious effects of failures in adjacent structural elements are accounted for by increased stress levels in the critical elements. Multi-Site Damage (MSD) refers to damage in which the stress intensity factors are correlated with the crack sizes at nearby stress raisers. Because these two types of damage at multiple sites require different approaches to the risk analyses, they are treated separately. Section 2 addresses MED while Section 3 addresses MSD damage. A summary of the Phase 1 effort is presented in Section 4.

## Section 2

### *Multi-Element Damage (MED)*

---

When the interactive effects of the structural integrity of adjacent structural elements are accounted for only by increased stress levels due to element failure, the resulting damage is characterized as multi-element damage (MED). In principle, the probabilities of failure in such scenarios can be quantified using multiple runs of PROF if the required input data are available. This is accomplished by calculating the conditional failure probabilities for each potential combination of failed and unfailed states of the elements. The unconditional failure probability of the composite structure is then a weighted average of the conditional probabilities where the weights are the probabilities of the composite structure being in each of the combinations. Since the calculations are most easily demonstrated by an example, the following subsections present the application of PROF to a three-element problem using data from the C-141 aircraft.

#### **2.1 Example Application of PROF to a Three-Element Structure**

Failure occurs at WS405 in the C-141 airframe when the chordwise joint fractures. Since the stress levels in the chordwise joint are dependent on the intact or failed status of both a splice fitting and a beam cap, the risk analysis for WS405 must combine conditional fracture probabilities for the relevant combinations of the states of the structural details. The probability of failure at this wing station under routine operations was previously calculated by Lockheed Aeronautical Systems Company (LASC) for a single inspection interval at 31,000 spectrum hours [2]. Because of the extensive analyses performed by LASC in their evaluation of the failure risks at WS405, most of the PROF input data were immediately available.

LASC performed extensive finite element analyses of the chordwise joint, splice fitting and beam cap at WS405 of the C-141 airframe. The intact or fractured status of the beam cap affects the stress levels in both the splice fitting and the chordwise joint. The intact or fractured status of the splice fitting also affects the stress levels in the chordwise joint. Thus, different crack growth life data (a versus T) and different maximum stress per flight distributions are needed for the various combinations of intact and fractured beam caps and splice fittings. (These

effects of the beam cap and splice fitting status are shown in the following subsection.)

Since structural failure at WS405 of the C-141 airframe occurs when the chordwise joint fractures, LASC established a fault tree which isolated the fracture events that need to be evaluated in the calculation of the probability of failure of WS405. This fault tree was restructured to demonstrate that the WS405 failure probability can be modeled as a weighted average of the probability of fracture of the chordwise joint given the status of the splice fitting and the beam cap. The weighing factors are the probabilities of the intact or fractured status of the splice fitting and the beam cap.

The chordwise joint fracture can be visualized in terms of the Venn diagram of Figure 1 in which the event of failure is partitioned into four mutually exclusive sub-events. The probability of failure at WS405 (POF) is then given by:

$$\begin{aligned}
 \text{POF} &= P\{\text{CSF}, \text{SFTAC}, \text{BCTAC}\} + P\{\text{CSF}, \text{SFTAC}, \text{BCF}\} \\
 &\quad + P\{\text{CSF}, \text{SFF}, \text{BCTAC}\} + P\{\text{CSF}, \text{SFF}, \text{BCF}\} \\
 &= P\{\text{CSF} \mid \text{SFTAC}, \text{BCTAC}\} \cdot P\{\text{SFTAC}\} \cdot P\{\text{BCTAC}\} \\
 &\quad + P\{\text{CSF} \mid \text{SFTAC}, \text{BCF}\} \cdot P\{\text{SFTAC}\} \cdot P\{\text{BCF}\} \\
 &\quad + P\{\text{CSF} \mid \text{SFF}, \text{BCTAC}\} \cdot P\{\text{SFF}\} \cdot P\{\text{BCTAC}\} \\
 &\quad + P\{\text{CSF} \mid \text{SFF}, \text{BCF}\} \cdot P\{\text{SFF}\} \cdot P\{\text{BCF}\}
 \end{aligned} \tag{1}$$

where

CSF = chordwise joint fracture

SFTAC = splice fitting intact

SFF = splice fitting fractured

BCTAC = beam cap intact

BCF = beam cap fractured

$P\{A, B, C\}$  = Probability of events A and B and C

$= P\{A \mid B, C\} \cdot P\{B\} \cdot P\{C\}$

$P\{A \mid B, C\}$  = Conditional probability of event A given the events B and C

Time histories of the conditional probability of chordwise joint fracture given the intact or failed status of the splice fitting and beam cap can be calculated by PROF (using the appropriate  $a$  versus  $T$  and maximum stress per flight distribution). Similarly, the time histories of the probability of the splice fitting and beam cap being in an intact or failed status can also be calculated by PROF. These numbers are then combined to calculate the unconditional probability of WS405 failure.

It might be noted that the example results are stated in terms of one location on the C-141 aircraft. There are two locations (right and left wings) on each of about 265 airframes that are susceptible to the risks modelled in the analyses. The risk per airframe and the risk to the entire fleet can be calculated from the formulas:

$$POF_{A/C} = 1 - (1 - POF)^2 \quad (2)$$

$$POF_{FLEET} = 1 - (1 - POF_{A/C})^{265} \quad (3)$$

### 2.1.1 PROF Input Data for Example Three-Element Structure

The list of inputs required for PROF is presented in Table 1. All but the repair quality distribution, the standard deviation of fracture toughness, and the Gumbel fit to the maximum stress per flight distribution were supplied by LASC. The following description of the input data is in the same order as that of Table 1.

Figure 2 presents the stress intensity factor coefficient as a function of crack size ( $K/\sigma$  versus  $a$ ) for the three structural details. The data files for all three elements extended to larger crack sizes but (as will be shown) rapid, unstable crack growth for all three elements begins to occur before the cracks reach 1 in. Cracks in the splice fitting and the beam cap jump holes at about 0.35 in. The  $K/\sigma$  at the two sides of the hole are connected by a straight line. As will be discussed, these crack size regions were deleted for the analyses. (Note that as the crack restarts on the other side of the hole, the crack measurement position is changed.)

**TABLE 1**  
**LIST OF PROF INPUT DATA**

	NATURE	FORMAT
<b>Material/Geometry</b>		
K/ $\sigma$ vs a	Deterministic	Data File
K <sub>c</sub>	Stochastic	Parameters (Normal)
<b>Aircraft/Usage</b>		
Analysis Locations		Constants
a vs T	Deterministic	Data File
MAX $\sigma$ per Flight	Stochastic	Parameters (Gumbel)
Initial Crack Sizes	Stochastic	Data File
<b>Inspection/Repair</b>		
Times	Deterministic	Constants
Inspection Capability	Stochastic	Parameters (Lognormal)
Repair Quality	Stochastic	Data File

The mean and standard deviation of fracture toughness for the 7075-T6 details are presented in Table 2. PROF assumes that fracture toughness has a normal distribution. The standard deviations were obtained by assuming that fracture toughness determinations have a 5 percent coefficient of variation, i.e.,  $\mu/\sigma = 0.05$ . For the conditions of this study, the probability of fracture was not sensitive to the assumed coefficient of variation.

**TABLE 2**  
**PARAMETERS FOR DISTRIBUTION OF FRACTURE TOUGHNESS**

DETAIL	$\mu$ (KSI $\sqrt{\text{IN.}}$ )	$\sigma$ (KSI $\sqrt{\text{IN.}}$ )
CHORDWISE JOINT	59.4	3.0
SPLICE FITTING	53.6	2.7
BEAM CAP	65.0	3.2

Crack growth as a function of spectrum hours (a versus T) is presented in Figures 3, 4, and 5 for the chordwise joint, splice fitting and beam cap, respectively. There are four a versus T curves for the chordwise joint representing the four conditions of the splice fitting and the beam cap being intact or fractured. The chordwise joint a versus T curve with the splice fitting intact and the beam cap failed, Figure 3, is identical to that with both the splice fitting and the beam cap intact. (The maximum stress per flight distribution on the chordwise joint with the splice fitting intact and the beam cap failed is, however, more severe than that with both the beam cap and splice fitting intact.) These curves were truncated at the crack size for which the next flight would have produced fracture.

Figure 4 displays a versus T for the splice fitting with the beam cap intact and fractured. Figure 5 displays a versus T for the beam cap. The state of the splice fitting does not effect crack growth in the beam cap. The vertical jumps in the curves represent the jump in crack size as cracks in these details instantaneously cross holes. In principle, such jumps should be successfully modelled by PROF. In practice, the jump increments had to be removed because they caused the introduction of extraneous meshes for the tabled crack size distributions and created numerical integration inconsistencies.

The maximum stress per flight data and the Gumbel distribution fits (assumed by PROF) are presented in Figures 6, 7, and 8 for the chordwise joint, splice fitting, and beam cap, respectively. The Gumbel fits were quite adequate at the high stress levels which are the most significant in the calculation of fracture probability.

The crack size distributions were derived by LASC from inspection data and were provided as parameter values for the Weibull distribution. The crack size distributions were derived to model the cracks that would be in the structural details at 31,000 spectrum hours, the zero reference time for the risk analyses. The Weibull parameters are presented in Table 3 and the cumulative distribution functions for all three elements are shown in Figure 9. Note that about 70 percent of the beam caps have cracks greater than 1 in. at 31,000 hours, i.e., more than 70 percent of the beam caps are in a failed state at the start of the analyses. The original PROF code had to be modified to handle the integrations over these large crack sizes.

**TABLE 3**  
**WEIBULL CRACK SIZE PARAMETERS**

DETAIL	SCALE PARAMETER ( $\beta$ ) (in.)	SHAPE PARAMETER ( $\alpha$ )
CHORDWISE JOINT	0.2456	2.09
SPLICE FITTING	0.1750	1.21
BEAM CAP	2.5300	1.19

The zero reference time for the analyses was 31,000 spectrum hours. This reference time was set to agree with the initiating crack size distributions in the elements. The inspection interval was set at 328 hours. Risk analyses were performed both with and without an inspection at the zero reference time. The average flight length was 3.5 hours.

Inspections were performed using x-rays and the capability of the inspections was defined to be that as determined by the "Have Cracks Will Travel" program [3]. Figure 10 shows the data points and the cumulative lognormal fit to the probability of detection function. The parameters of the fit are  $a_{50} = 0.445$  in. ( $\mu = -0.810$ ) and  $\sigma = 0.94$ . For this inspection the probability of detecting a crack of size 0.445 in. is 0.5. LASC used a different but equivalent fit to these data.

The assumed equivalent repair flaw size distribution was a Weibull distribution with scale parameter ( $\beta$ ) equal to 0.010 in. and shape parameter ( $\alpha$ ) equal to 1.0. These equivalent repair crack sizes are small (almost good as new) compared to the initial crack size distributions and essentially removed the repaired structural elements from the analysis.

### 2.1.2 Probabilities of Fracture for Example Three Element Structure

PROF computes the single flight probability of fracture at ten approximately equally spaced times throughout each usage interval. Usage intervals are specified in terms of spectrum hours from the zero reference time and define the times at which the inspection and repair actions



are taken. In this risk evaluation at WS405 of the C-141, the analyses were performed over two usage intervals of 328 hour duration. The analyses were run with no inspection at  $T = 0$  (31,000 spectrum hours) and starting with an inspection at  $T = 0$ .

PROF also calculates interval probability of fracture but only at the end of a usage interval. For the structural elements and conditions of this study, the probability of fracture was dominated by cracks reaching unstable size (about 1 in.) as opposed to an encounter of a maximum stress in a flight. That is, the probability of fracture was determined primarily from the distributions of crack sizes. As a result, the single flight and interval probability of fracture were equal (to three significant figures) for the chordwise joint and the beam cap. The interval probabilities of fracture for the splice fitting were about five percent greater than the single flight fracture probabilities. Therefore, in this application the single flight fracture probabilities can be used for the probabilities of intact and fractured status of the splice fitting and beam cap (Equation 1) in calculating the unconditional probability of failure at the ten times in a usage interval. This topic will be addressed further in subsection 2.2.

With no inspection/repair cycle at the start of analysis, Figure 11 presents the conditional single flight probability of failure of the chordwise joint given the intact or fractured status of the splice fitting and beam cap. The unconditional failure probability is a weighted average of these conditional probabilities with the weights being determined by the proportion of intact and failed splice fittings and beam caps.

Figure 12 presents the probability of fracture as a function of spectrum hours for the splice fittings and the beam caps when the analysis is started without an inspection, i.e., the first inspection is performed at 328 hours. The very high fracture probabilities for the beam caps reflect the very high proportion of large cracks (fractured beam caps) in the initial conditions. The inspection/repair cycle at 328 hours replaced the fractured beam caps and greatly reduced the fracture probability for this element. The effect of the failed beam cap on the fracture probability of the splice fitting was relatively minor in comparison to other effects.

Although the fracture probabilities of Figure 12 were calculated as the probability of the

element fracturing in a single flight, these values are essentially equal to the interval probabilities of fracture, i.e., the probability of fracture between time zero (or the inspection at 328 hours) and the spectrum hours at the time of the calculation. As noted earlier, this equivalence of the single flight and interval probabilities is a result of the fracture probabilities for these elements being driven by the percentage of cracks reaching unstable size rather than the occurrence of a single large stress. Thus, the probabilities of the intact or fractured status of the splice fitting and beam cap as given in Figure 12 were used in Equation 1 to calculate the unconditional failure probability of the chordwise joint.

The dashed line of Figure 13 is the unconditional failure probability of the chordwise joint with no inspection at the start of the analysis. This probability is superimposed on the conditional failure probabilities of Figure 11. After the inspection/repair cycle at 328 hours, the unconditional failure probability is essentially equal to the conditional failure probability given that the splice fitting and beam cap are intact.

To determine the effect of performing an inspection/repair cycle at  $T = 0$  (31,000 hours), the complete analysis was performed by specifying that the first inspection/repair cycle was at  $T = 0$  (31,000 hours) with subsequent inspection/repair cycles at 328 hour intervals. Figure 14 compares the unconditional chordwise joint failure probabilities for the two inspection scenarios. As expected, eliminating the failed splice fittings and beam caps significantly improves the failure risks.

## **2.2 Discussion of PROF Multi-Element Analysis**

The previous example demonstrates that PROF can be used to evaluate the fracture risks associated with more complex structures than the single stress raiser which is the current basis of the calculations. However, in performing the example analysis many individual PROF runs were required, the results of the individual runs were downloaded to a personal computer, and the results were combined using a spreadsheet program. To automate this process will require a post-processor for combining the results of the individual runs as part of a multi-element risk analysis. The PROF initiating routine will also require modification to define the post-processing analyses. As a practical matter, the number of interacting elements in a single analysis will be

limited by the amount of available input data.

The weight factors for combining the conditional probabilities of failure (see Equation 1) are the unconditional probabilities that the interacting elements are in failed or unfailed states. The exact values of these weight factors would be given by PROF's interval probabilities. However, as PROF is currently structured, the interval probabilities are only calculated at the beginning and end of usage intervals and not at the ten intermediate times of the single flight PROF calculations. Prior to the application to multi-element damage, the interval probabilities were only used in the estimation of expected costs of failure and maintenance. The PROF code can be modified to calculate the interval failure probabilities at the intermediate times but a large increase in computer time will be required to perform the calculations.

## Section 3

### *Multi-Site Damage (MSD)*

---

Multi-site damage (MSD) is generally associated with many neighboring cracks along a row of rivets (fastener holes) in the fuselage or wing structure and has been widely discussed over the last several years [4-9]. Summaries of the damage tolerance approach to this problem are discussed by Lincoln [10] for commuter aircraft and by Swift [11] for commercial aircraft. Early evaluations of the effect of multiply cracked structures were conducted by Brussat and coworkers [12,13], Broek [14], Karlsson and Backlund [15], and Burck and Rau [16] for single and multi-site cracks. Brussat introduced the use of the compounding method, whereby known solutions are combined using the product of the different geometrical factors, to obtain approximate solutions. In general, the early investigators [9-13] reported stress intensity factor results primarily for multi-site cracks emanating from fastener holes in infinite plate configurations. More recently, Nishimura, Noguchi and Uchimoto [17] discussed their compounding method for estimating stress intensity factors for multi-site cracks emanating from a row of fastener holes located perpendicular to the loading direction in a finite plate. The finite element and boundary element techniques also have been used to estimate the stress intensity factor for complex structures. Overviews of finite element and analytical methods are given by Atluri [18] and Actis and Szabo [19]. A number of investigators [20-22] have used the finite element method to solve multi-site damage problems. Recently, Dawicke and Newman [23] have discussed an alternating indirect boundary element (AIBE) technique, which can be incorporated into a fatigue growth prediction code.

MSD is distinguished from multi-element damage by the fact that in MSD the stress intensity factors for cracks associated with one stress raiser are dependent on the size of nearby cracks. Given a specified set of cracks in a geometric configuration, the stress intensity factor for the dominant crack can be calculated. In theory, crack growth of the dominant crack can also be calculated and workable methodologies for this calculation are under development. Risk analysis, however, must also account for the random nature of the initiation and growth of the dominant crack as well as the cracks in nearby structure.

PROF can be applied to MSD problems by defining a few MSD cracking scenarios which will provide reasonable bounds on the probability of fracture. If the cracking scenarios reasonably cover all possibilities and the probability of occurrence of each scenario is known, a weighted average of the probabilities of failure over the scenarios will yield a reasonable estimate of the overall failure probability. Since realistic MSD scenarios will require multiple crack size versus time curves to account for the changing sizes of cracks in nearby structure, a dynamic interface with a crack growth program may be required for efficient computations.

Prior to applying PROF to MSD scenarios, a study was undertaken to review available data and literature and to determine the effect on crack coalescence of: (a) the influence of crack sizes on the predicted strength levels for link-up (i.e., the coalescence strength) and (b) the influence of the spacing between adjacent crack tips. The influence of three fracture criteria on the characterization of residual strength was also determined. The crack configurations considered were: a) single crack; b) two unequal length collinear cracks; c) three collinear cracks; and, d) a periodic array of collinear cracks. The various crack configurations are illustrated in Figure 15 and were assumed to be in an infinite sheet subjected to uniform, uniaxial tensile stress. The fracture criteria were Irwin's fracture criterion, the Swift plastic zone interaction criterion, and a two parameter R-curve criterion. This subsection presents the results of this study.

### 3.1 Geometric Parameters

In the analysis of a multiple crack system (see Figure 15 a,c,d), the geometric parameters are (a)  $a/b$ , the ratio of long crack size to short crack size and (b)  $\omega/d$ , the ratio of the distance between adjacent crack tips to the periodic spacing of the cracks. Table 4 lists the values of these parameters chosen for the different crack configurations employed in this study.

The foundation for all analysis conducted in the study was the linear elastic fracture mechanics parameter  $K$ , i.e., the stress intensity factor. The stress intensity factor can in general be described using

$$K = \sigma \sqrt{\pi a} \quad (4)$$

where  $\sigma$  is the remotely applied stress,  $\beta$  is the geometry factor and  $a$  is the crack length. For a single crack in an infinite sheet (Figure 15b),  $\beta = 1$ . The expressions for  $\beta$  corresponding to two collinear cracks, three collinear cracks and a periodic array of collinear cracks, in an infinite sheet are given by Rooke and Cartwright [26]. Using the values for  $K$  for each of the crack tips shown in Figure 15, the crack tip location of the highest driving force was determined. These locations are indicated in Table 4.

**Table 4. Geometric Parameters for Different Crack Configurations**

Crack System	Figure 15	Critical location for failure	$\omega$ (inch)	$d$ (inch)	$a/b$	$a$ (inch)	$b$ (inch)
Periodic array of Collinear Cracks	a	A = B	0.05 0.10 0.25 0.50	1	1	0→0.5	0→0.5
Single Crack	b	A = B	-----	-----	-----	0→0.5	-----
Two Collinear Cracks	c	B	0.05 0.10 0.25 0.50	1	1→10	0→0.5	0→0.05
Two Collinear Cracks	c	B	0.05 0.10 0.25 0.50	1→50	- **	0→48	0.25
Three Collinear Cracks	d	B	0.05 0.10 0.25 0.50	1	1→10	0→0.5	0→0.05
Three Collinear Cracks	d	B	0.05 0.10 0.25 0.50	1→50	**	0→48	0.25

\*\*  $a/b$  ratio is not a variable

Initial studies evaluated the influence of the crack sizes and fracture criteria, on residual strength levels for the multiple crack configurations identified in Figure 15. The periodic spacing

parameter,  $d$ , was set equal to 1 inch, a typical fastener spacing. Other geometric variables were varied depending of the configuration being analyzed. In the early studies, the size of the uncracked ligament  $\omega$  (i.e., the distance between the adjacent crack tips), was varied from 0.05 inch to 0.95 inch. The crack size parameter  $a/b$  was varied from 1 to 10, so that the crack size  $a$  varied from 0.025 to a maximum of 0.475 inch. In later studies, to determine the influence of a short crack on the residual strength of a longer crack, the half -length ( $b$ ) of the short crack in Figures 15 c and d was fixed to 0.25 inch. The long crack half length ( $a$ ) was varied from 0.025 inch to 48 inches.

### 3.2 Influence of Crack Size

Figure 16 presents the variation of residual strength level as a function of crack size for two extremely different crack geometries. These results are based on the Irwin fracture hypothesis and assume a plane stress fracture toughness ( $K_{IC}$ ) of 60 ksi $\sqrt{\text{in}}$ . In the figure, the link-up process for the infinite collinear array of cracks (with  $d=1$ ) is shown to reduce the residual strength drastically when compared to the residual strength of a single crack of the same length. Note that comparisons are only valid for strength levels below the (arbitrarily selected) yield strength and, when the crack half-length in the periodic array is 0.5 inch, the cracks are linked. For the periodic array configuration, when the cracks coalesce, the structure fails, so the coalescence strength is equal to the residual strength.

Figure 17 compares the coalescence strength behavior for all multiple crack geometries where the distance between cracks is  $d$  ( $= 1$  inch). The curves for single and infinite collinear crack configurations were taken from Figure 16. In Figure 17, the points on the curves associated with the two and three collinear crack geometries are based on constant values of the uncracked ligament parameter  $\omega$ . These curves represent ratios between the crack lengths ( $a/b$ ) that range from 1 to 10. For  $a/b = 1$ , the crack lengths are all equal, and for the two and three collinear crack curves, the ( $a/b = 1$ ) points are located on the left.

In Figure 17, the coalescence strength level for any number ( $> 2$ ) of equal size collinear cracks, is bounded between the two equal collinear cracks and the infinite collinear crack configuration. For values of  $\omega > 0.1$  inch, the coalescence strength decreases with increase in  $a/b$  ratio and for values of  $\omega \leq 0.1$  inch, the coalescence strength remains essentially constant.

The interaction between a long crack and a short crack in terms of the coalescence strength levels (increase/decrease) is decided by the value of the size of the uncracked ligament  $\omega$ .

The importance of physical crack size in explaining the link-up of a short crack with the long crack has been addressed previously [20,21]. In these previous studies, a physical mechanism by which the shorter cracks grow faster than the long crack could not be identified. The analyses of this study (Figure 17) indicate that the ratio of  $\sigma_A(\text{after})/\sigma_A(\text{before})$  is not affected by the increasing crack size,  $a$ . Rather, the distance  $\omega$  between the adjacent crack tips is identified as the more important variable than the physical size of the individual cracks as the crack tips converge.

### 3.3 Influence of the Longest Crack Size

In this subsection, the shorter crack half-length  $b$  in the two and three crack configurations is kept fixed ( $=0.25$  inch) and the larger crack half-length  $a$  is varied for several fixed values of  $\omega$ . The analytical results are based on Irwin fracture hypothesis, (see subsection 3.4.1) taking  $K_{cr} = 60 \text{ ksi}\sqrt{\text{in}}$ . The coalescence strength,  $\sigma_{cs}$ , is associated with the stress intensity factor at location B, the tip of the longest crack in the multi-crack system.

#### 3.3.1 Two Crack Configuration

Figures 18 and 19 present the ratio of the coalescence strength ( $\sigma_B$ ) to the strength levels associated with extending crack tip A ( $\sigma_A$ ) and crack tip D ( $\sigma_D$ ) for a two crack configuration. The following observations are made from Figure 18 which describe the relative strength levels required to extend the cracks at positions A, B, and D. Before crack coalescence, the strength ratio level ( $\sigma_A$  or  $\sigma_B$ ) required to extend the tips of the longest crack is not affected by increasing the crack size  $a > 1$  inch. The ratio between the coalescence strength and the residual strength at location A ( $\sigma_B/\sigma_A$ ) is greater than the ratio between the coalescence strength and the residual strength at location D ( $\sigma_B/\sigma_D$ ) (see Figure 19); and, the strength,  $\sigma_D$ , is higher than the strengths  $\sigma_A$  or  $\sigma_B$ . This implies that the critical location for crack link-up or failure is at location B ( $\sigma_B < \sigma_A < \sigma_D$ ), as indicated in Table 5. Increasing the long crack size,  $a$ , for a fixed short crack size,  $b$ , the residual strength  $\sigma_D$  remains fairly constant, but the strength ratio ( $\sigma_B/\sigma_A$  or  $\sigma_B/\sigma_D$ ) levels is a function of uncracked ligament size  $\omega$ . Decreasing  $\omega$  decreases the strength ratio,



$\sigma_B/\sigma_A$ , because the coalescence strength decreases by 40 to 50% of the strength corresponding to the crack tip at location A. This shows that  $\omega$  is the parameter which establishes the strength ratio.

**Table 5. A Summary of Critical Crack Location and Coalescence Strength**

Crack System	Figure 1	Critical crack tip location for link-up	Next most critical crack tip location for residual strength	Remarks	Residual strength levels
Infinite Series of Cracks	a	A = B	---	Coalesce strength $\leq$ Residual strength	Lower Bound
Single Crack	b	A = B	---	No coalescence	Upper Bound
Two Collinear Cracks	c	B for $a > b$	A for $a > b$	Coalesce strength $\leq$ Residual strength for $\omega \leq 0.1$ inch	refer to remarks
Three Collinear Cracks	d	B for $a > b$	D for $a > b$	Coalesce strength $\leq$ Residual strength for $\omega \leq 0.1$ inch	refer to remarks

During coalescence the crack tips B and C merge (Figure 15). The residual strength  $\sigma_A$  after coalescence is now a square root function of the initial crack spacing  $d$ . Figure 20 describes the ratio of coalescence strength to the residual strength after crack link-up. The figure implies that when  $\sigma_B$  (before)/ $\sigma_A$ (after)  $> 1$ , complete fracture of the plate occurs immediately after coalescence. Fracture immediately after coalescence will occur for various combinations of  $a$ ,  $b$ , and  $\omega$ . However, for  $\omega \leq 0.1$  inch and for any values of  $a$  greater than about 6 inches, the strength ratio,  $\sigma_B$ (before)/ $\sigma_A$ (after), remains fairly constant. This means that increasing (or decreasing) the value of  $\omega$  by 15%, the value of the crack half-length  $a$  must be decreased by 1% to make the strength ratio,  $\sigma_B$  (before)/ $\sigma_A$ (after), remain constant. Thus, the half-length  $a$  of the long crack does not significantly influence the decrease in the coalescence strength to residual strength ratio ( $\sigma_B/\sigma_A$  (after)). As  $\omega$  becomes smaller, Figure 20 illustrates that after coalescence, the crack will not extend to failure without an increase in load.

Figure 21, illustrates the effect of the largest crack size on the residual strength ratio (before/after) for crack tip A. When a short crack is interacting with another short crack, the reduction in the residual strength is much greater than when a long crack is interacting with a

short crack. For example, the strength condition for growth of crack tip A before coalescence is approximately 1% higher than that after coalescence for  $a > 10$  inch. Another observation here is that if the coalescence stress ( $\sigma_B$ ) is less than the residual strength at crack tip A before coalescence then the crack will be stable after coalescence.

### 3.3.2 Three Crack Configuration

Analyses similar to the above were also performed for the three crack configuration. In Figure 22, the coalescence strength,  $\sigma_{cs}$ , is associated with the stress intensity factor at locations A and B, the tip on either side of the longest crack in a three crack system (see Figure 15d). The following observations are made from Figure 22 with regard to the strength ratios plotted which describe the relative strength levels required to extend the cracks at positions B and D. Before crack coalescence, the strength level ( $\sigma_A$  or  $\sigma_B$ ) required to extend the tips of the longest crack and the strength level required to extend the crack tip D ( $\sigma_D$ ) are hardly affected by increasing the crack size for  $a > 3$  inch. Since  $\sigma_C < \sigma_D$ , the ratio between the coalescence strength and the residual strength at location D ( $\sigma_B/\sigma_D$ ) is greater than the ratio between the coalescence strengths at location B or C; and, the strength,  $\sigma_D$ , is higher than the strengths  $\sigma_B$  or  $\sigma_C$ . This dictates that the critical location for crack link-up or failure is at location B ( $\sigma_B = \sigma_A < \sigma_C < \sigma_D$ ), as indicated in Table 5.

During coalescence the crack tips B and C merge. The residual strength,  $\sigma_D$ , is now a square root function of  $d+b$ . The residual strength,  $\sigma_B$ , before coalescence remains fairly constant for  $a > 3$  inch, whereas the residual strength,  $\sigma_D$ , after coalescence shows a strong decreasing dependence on the periodic spacing parameter  $d$ . Because of this, the strength ratio,  $\sigma_B/\sigma_D$ , is a decreasing function of crack size  $a$  for  $\omega \leq 0.25$  inch, as shown in Figure 22. Also, as seen in Figure 23, the residual strength,  $\sigma_D$ , after coalescence is approximately 15% higher than that of before coalescence for  $a > 10$  inch. Another observation here is that if the coalescence stress ( $\sigma_B$ ) is equal to the residual strength at crack tip D before coalescence then the crack will be unstable after coalescence.

### 3.4 Influence of Fracture Criteria and Material Properties

The residual strength levels associated with crack coalescence were calculated and compared as a function of three different fracture criteria. The criteria were based on (a) the Irwin fracture hypothesis or critical stress intensity factor,  $K_{cr}$ , approach; (b) the Swift plastic zone interaction model, and, (c) a two parameter R-curve analysis. The fracture criteria are defined in Subsection 3.4.1 and the results of the comparative are presented in Subsection 3.4.2

#### 3.4.1 Fracture Criteria

**(a) Irwin Fracture Hypothesis:** The residual strength based on thin sheet abrupt fracture can be written in the form

$$K = K_{cr} \quad (5)$$

where  $K$  is obtained from Eq. 4 for a given crack configuration and  $K_{cr}$  is determined from standard laboratory tests. For a thin sheet, the fracture toughness  $K_{cr}$  can be a function of sheet thickness. The criterion for crack coalescence is the highest  $K$  for adjacent crack tips.

**(b) Swift Plastic Zone Interaction Model:** Net section yielding stresses for the presence of multiple cracks are calculated based on the asymptotic formula for the stress near a crack tip,

$$r_p = (1/2\pi)(K/\sigma_{ys})^2 \quad (6)$$

where  $\sigma_{ys}$  is the yield strength,  $r_p$  is the plastic zone radius and  $K$  is the stress intensity factor at the crack tip. Swift's criterion for the linkup of two crack tips approaching each other in terms of the distance  $\omega$  between the adjacent crack tips is (see Figure 24):

$$\omega = r_{yB} + r_{yC} \quad (7)$$

where  $r_{yB}$  and  $r_{yC}$  are the radii of the plastic zones at location B and C, respectively. Using Eqs. 6 and 7, Swift's criterion becomes:

$$\omega = 1/2\pi[(K_B/\sigma_{ys})^2 + (K_C/\sigma_{ys})^2] \quad (8)$$

where  $K_B$  and  $K_C$  are the stress intensity factors at the coalescing crack tips located at points B and C, respectively. For the crack configuration shown in Figure 24,  $a > b$ ,  $2a$  represents the length of the long crack (AB),  $2b$  represents the length of the short crack (CD) and  $d$  defines the crack spacing parameter (crack center to crack center). In terms of yield strength  $\sigma_{ys}$ , distance  $\omega$  between adjacent crack tips, crack half-lengths  $a$  and  $b$ , and geometry factors  $\beta_B$  and  $\beta_C$ , one can estimate the coalescence strength  $\sigma_{cs}$ ,

$$\sigma_{cs} = \sigma_{ys} [2\omega/(a\beta_B^2 + b\beta_C^2)] \quad (9)$$

The geometry factors  $\beta_B$  and  $\beta_C$  are associated with the points shown in Figure 24 and are given in [26] for the various crack geometries.

**(c) Two Parameter R-Curve Criterion:** The two parameter R-Curve criterion

$$K = K_R \quad (10a)$$

$$dK/da \geq dK_R/da \quad (10b)$$

is satisfied by equating the crack tip stress intensity factor  $K$  for each stress level to the resistance curve. Crack instability occurs when the rate of change of applied stress intensity ( $dK/da$ ) equals the rate of change of resistance ( $dK_R/da$ ).

In Figure 25, the  $\sigma$  curve represents the variation of  $K$  with the crack length for a fixed value of the applied stress  $\sigma$  and accounts for the effect of adjacent (growing) cracks when necessary. The relationship between the crack size and the stress intensity factor is

$$a = 1/\pi(K/\sigma\beta_B)^2 \quad (11)$$

The R Curve is obtained by varying the applied stress  $\sigma$  for a fixed value of  $\omega$ . The power-law relationship between the resistance stress intensity and increment in crack size is obtained from a curve-fit of the CTOA analytical data [22].

$$K_R = C(\Delta a)^n \quad (12)$$

The material properties C and n are given in Table 6.

**Table 6. Material Properties**

Properties	Simulated 2024-T3 Aluminum
Yield Strength, $\sigma_{ys}$	60±10 (ksi)
Plane Strain Fracture Toughness, $K_{IC}$	30 (ksi√in)
Plane Stress Fracture Toughness, $K_{cr}$	60 (ksi√in)
Resistance Curve, $K_R$	124 ( $\Delta a$ ) <sup>0.224</sup> (ksi√in)

The intersection point in Figure 25 is obtained by iterating on  $\Delta a$  to maintain equality between K and  $K_R$  until Eq. 8b ( the dual criterion) is satisfied. The value of the final crack length  $a_f$  in terms of initial crack size  $a_i$  and crack growth increment  $\Delta a$  is

$$a_f = a_i + \Delta a \quad (13)$$

The expression for the coalescence strength is given by

$$\sigma_{cs} = \sigma_B = K_f / (\beta_B \sqrt{\pi a_f}) \quad (14)$$

### 3.4.2 Influence of Fracture Criteria

The strength levels associated with crack coalescence for infinite collinear cracks were calculated and compared for the three different fracture criteria and for selected yield strengths and fracture toughness, Figures 26, 27 and 28. In these analyses,  $d = 1$  which implies  $\omega = 1 - 2a$ . Figure 26 displays the coalescence strength levels for the three criteria for a material with yield strength of 60 ksi and a fracture toughness of 60 ksi√in. At this fracture toughness, the Irwin criterion is dominant for small cracks (larger sizes of the uncracked ligament) and the Swift criterion is dominant at the larger crack sizes (small values of the uncracked ligament). However, the fracture toughness has a significant effect on the Irwin criteria coalescence strength calculations as shown in Figure 27. Decreasing fracture toughness from 60 ksi√in to 30 ksi√in

decreased the residual strength by half. The sensitivity of coalescence strengths to the Swift plastic zone interaction model is shown in Figure 28. In general, these results show that at smaller crack sizes (larger  $\omega$ ), either the Irwin criteria or the R-Curve analysis provide the lower bound for the coalescence strength level. However, the Swift criteria becomes dominant when the size of the uncracked ligament becomes small.

The strength levels associated with crack coalescence for the two crack configuration are calculated and compared as a function of three different fracture criteria in Figures 29 and 30. In Figure 29, as two adjacent crack tips approach each other, the dominant criterion is based on R-Curve analysis as compared to Irwin's fracture hypothesis. Similarly, in Figure 30, as two adjacent crack tips approach each other, the dominant criterion is the Swift plastic zone interaction criterion as compared to the R-Curve analysis criterion.

### 3.5 Discussion of MSD Results

For cracks in an infinite plate:

- (1) For nearby cracks, the crack coalescence strength is largely independent of the largest crack size and its ratio to the crack with which it coalesces.
- (2) By adding a small crack ( $2b = 0.5$  inch) ahead of a larger crack of size  $2a$ , the reduction in the residual strength is greater than 10% for  $a < 2$  inches, and the reduction in the residual strength is less than 5% for  $a > 10$  inches.
- (3) The potential exists for immediate failure after coalescence occurs.
- (4) The effect of typical variations in fracture toughness on crack coalescence and residual strength levels is more severe than yield strength that associated with typical variations.
- (5) The lower bound for the residual strength is decided by fracture toughness or R-Curve criterion for large values of the uncracked ligament,  $\omega$ . As the value of  $\omega$  approaches zero, the plastic zone criterion dominates.
- (6) The observations for crack coalescence using three fracture criteria (a) Irwin fracture

hypothesis, (b) Swift plastic zone interaction model and (c) two parameter R-Curve analysis imply that crack coalescence is most heavily influenced by the distance  $\omega$  between the adjacent crack tips.

## Section 4

### *Summary*

---

In this first phase of a two phase study to develop a computer program for risk analysis of fatigue damage at multiple sites, the computer code PROF was demonstrated to be applicable to the multi-element damage (MED) problem. The application requires the damage tolerant analysis and crack size input for each of the relevant structural elements and for the relevant combinations of intact and failed conditions of the subcritical structural elements on the critical elements. The demonstration was performed incorporating the effects of two subcritical elements on the failure probability of the chordwise joint at WS405 of the C-141 airframe. The analysis required multiple PROF runs and considerable data manipulations to combine the output of the PROF runs. To generalize PROF to perform all of the analyses will require at least a preprocessor to define the number and combinations of input required for the multi-element analysis and a post-processor for efficiently combining the PROF output into the failure probabilities of the complex structure.

The application of PROF in the MSD area is not as clear. Since the largest crack in a lap joint will grow the fastest, the population of crack sizes to be modelled should be defined in terms of the largest crack in the zones of equivalent stresses. The sizes of the cracks in the holes immediately adjacent to the largest crack must be accounted for but several studies have indicated that the sizes of the cracks in more remote holes are not important drivers. Reasonable scenarios can be defined to bound the fracture probabilities given complete damage tolerant analyses and crack size data. Such data were not made available for this phase of the study. Since PROF calculates failure probabilities in terms of the Irwin fracture hypothesis only, modifications may be required to also incorporate either the R-Curve or the Swift plastic zone criteria. When realistic data become available, sensitivity studies on the failure probabilities should be performed to evaluate the real effects of the failure criteria. Pre- and post-processors will also be required for the efficient application of PROF to MSD type applications.



# Section 5

## References

---

1. Berens, A.P., Hovey, P.W., and Skinn, D.A., "Risk Analysis for Aging Aircraft Fleets, Volume 1 - Analysis," WL-TR-91-3066, Air Force Wright Laboratory, Wright-Patterson Air Force Base, OH, 45433-6553, October, 1991.
2. Cochran, J.B., Bell, R.P., Alford, R.E., and Hammond, D.O., "C-141 WS405 Risk Assessment," Proceedings of the 1991 USAF Structural Integrity Program Conference, San Antonio, Texas, December, 1991.
3. Lewis, W.H., Sproat, W.H., Dodd, B.D., and Hamilton, J.M., "Reliability of Nondestructive Inspections - Final Report," SA-ALC/MME 76-6-38-1, San Antonio Air Logistics Center, Kelly Air Force Base, TX, December, 1978.
4. Orringer, O., "How Likely is Multiple Site Damage?," Structural Integrity of Aging Airplanes, ed. by Atluri, S. N., Sampath, S. G. and Tong, P., Springer-Verlag, 1990.
5. Tong, P., Arin. D. Y., Jeong, R. and Greif, R., "Current DOT Research on The Effect of Multiple Site Damage on Structural Integrity," Proceedings of 1991 International Conference on Aging Aircraft and Structural Airworthiness, Washington, D. C., pp. 111-157, November 19-21, 1991.
6. Tong, P., Grief, R. and Chen, L., "Residual Strength of Aircraft Panels with Multiple Site Damage," Proceedings of the International Workshop on Structural Integrity of Aging Airplanes, Atlanta, pp.200-216, March 31-April 2, 1992.
7. Tong, P., Sampath, S. C. and Broek, D., "Aging Aircraft, Detection of MSD, and the Risk of Failure," ICAF Conference, pp. , Japan, 1991.
8. Newman, J. C. and Harris, C. E., "Fracture Mechanics Research at NASA Related to the Aging Commercial Transport Fleet," Aging Aircraft and Structural Airworthiness, Washington, D. C., pp. 75-91, November 19-21, 1991.
9. Harris, C. E. and Heyman, J. S., "Overview of NASA Research Related to the Aging Commercial Transport Fleet," Journal of Aircraft, Vol. 30(1), 1993.
10. Lincoln, J. W., "Damage Tolerance for Commuter Aircraft," Proceedings of 1991 International Conference on Aging Aircraft and Structural Airworthiness, Washington, D. C., pp. 187-196, November 19-21, 1991.
11. Swift, T. "Important Considerations in Commercial Aircraft Damage Tolerance," Int. J. of Vehicle Design, Vol. 7(3-4), pp. 264-287, 1986.

12. Brussat, T. R., Chiu, S. T. and Creager, M., "Flaw Growth in Complex Structure," AFFDL-TR-77-79, Vol. 1, December, 1977.
13. Brussat, T. R., Chiu, S. T. and Rudd, J. L., and Creager, M., "Fatigue Crack Growth in Reinforced Panels with Initial Corner Crack," J. Engineering Fracture Mechanics, Vol. 14(4), pp. 665-683, 1981.
14. Broek, D., "Cracks at Structural Holes," MCIC-75-25, Metals and Ceramics Information Center, Columbus, Ohio, March 1975.
15. Karlsson, A. and Backlund, J., "Summary of SIF Design Graph for Cracks Emanating from Circular Holes," Int'l J. of Fracture, Vol. 14(6), pp. 585-596, 1978.
16. Burck, L. H. and Rau, C. A., "Fatigue Crack Propagation from Small Holes in Linear Arrays," Int'l J. of Fracture, Vol. 9(1), pp. 43-51, 1973.
17. Nishimura, T., Noguchi, Y. and Uchimoto, T., "Damage Tolerance Analysis of Multiple-Site Cracks Emanating From Hole Array," Journal of Testing and Evaluation, JTEVA, Vol. 18 (6), pp.401-407, 1990.
18. Atluri, S. N., "Simplified Computational Methods for Elastic and Elastic-Plastic Fracture Problems," Proceedings of 1991 International Conference on Aging Aircraft and Structural Airworthiness, Washington, D. C., pp. 407-453, November 19-21, 1991.
19. Actis, R. L. and Szabo, B. A., "Computation of Stress intensity Factors for Panels with Multi-site Damage," Technical Note WU/CCM-92/3, December, 1992.
20. Beuth Jr., J. L. and Hutchinson, J. W., "Fracture Analysis of Multi-site Cracking in Fuselage Lap Joints," Proceedings of the International Workshop on Structural Integrity of Aging Airplanes, Atlanta, pp. 47-60, March 31-April 2, 1992.
21. Park, J. H. and Atluri, S. N., " Fatigue Growth of Multiple-Cracks Near a row of Fastener -Holes in a Fuselage lap-Joints," report No. 92-1, December, 1992.
22. Newman Jr., J. C., Dawicke, D. S. and Bigelow, C. A., "Finite-Element Analysis and Fracture Simulation in Thin-Sheet Aluminum Alloy," Proceedings of the International Workshop on Structural Integrity of Aging Airplanes, Atlanta, pp. 47-60, March 31-April 2, 1992.
23. Dawicke, D. S. and Newman Jr., J. C., "Analysis and Prediction of Multiple-Site Damage (MSD) Fatigue Crack Growth," NASA Technical Paper 3231, August 1992.
24. Gallagher, J.P., Giessler, F.J., Berens, A.P., and Engle, R.M., "USAF Damage Tolerant Design Handbook: Guidelines for the Analysis and Design of Damage Tolerant Aircraft Structures," AFWAL-TR-82-3073, Flight Dynamics Laboratory, Wright-Patterson AFB, OH , May, 1984.

25. Swift, T. "Damage Tolerance Capability," FAA, Presented at Specialists Conference on Fatigue of Aircraft Materials, Delft University of Technology, Delft-The Netherlands, October 14-15, pp. 15, 1992.
26. Rooke, D. P. and Cartwright, D. J., "Compendium of stress Intensity Factors," Her Majesty's Stationary Office, London, 1976.

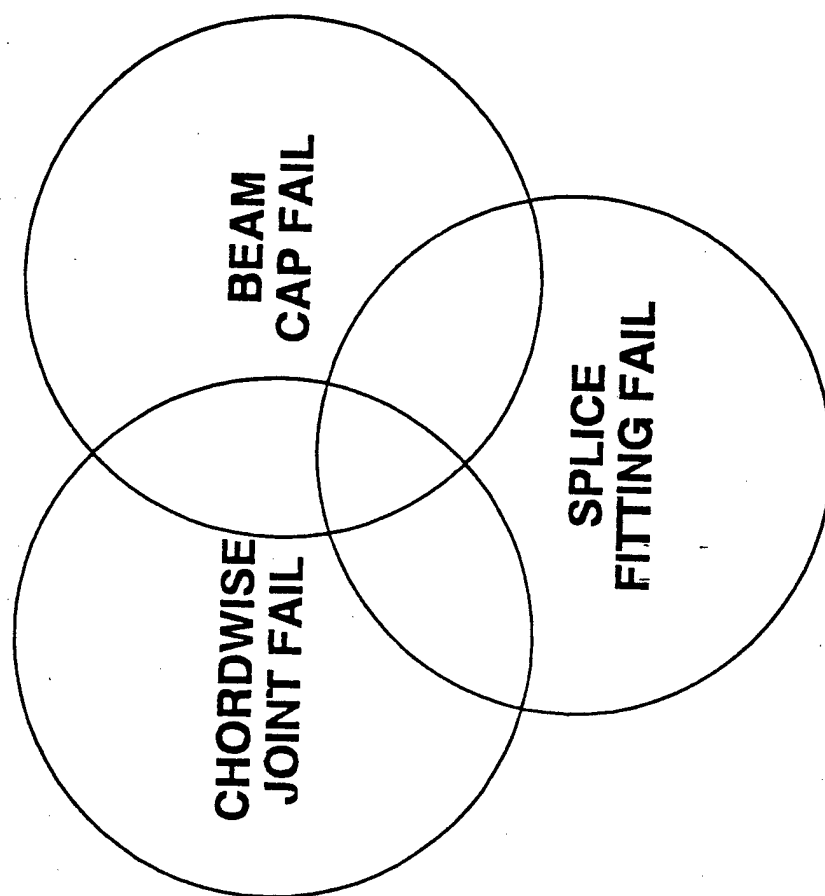


Figure 1 Venn Diagram Partitioning the Event of Chordwise Joint Failure.

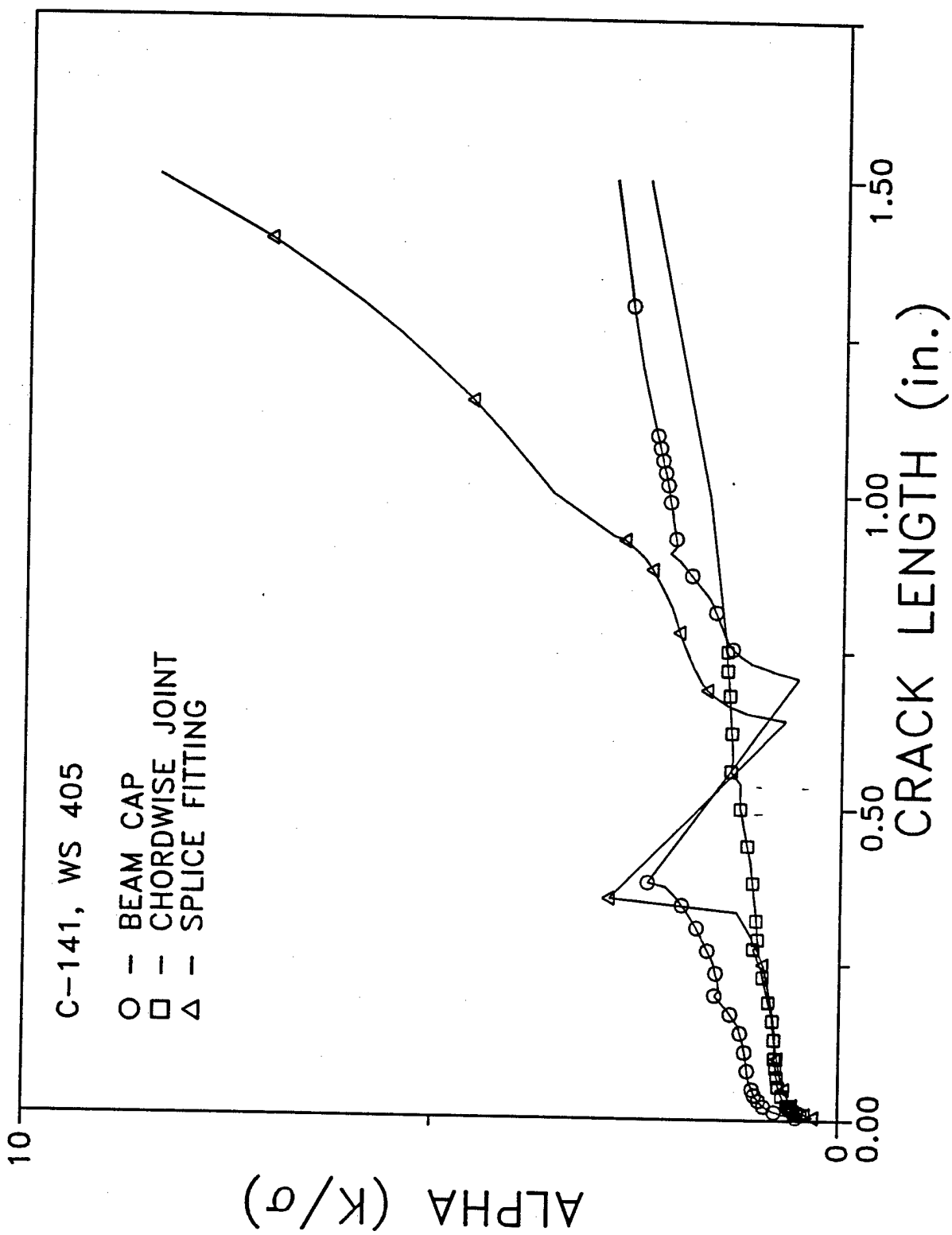


Figure 2  $K/\sigma$  Versus Crack Length for WS405 Structural Elements.

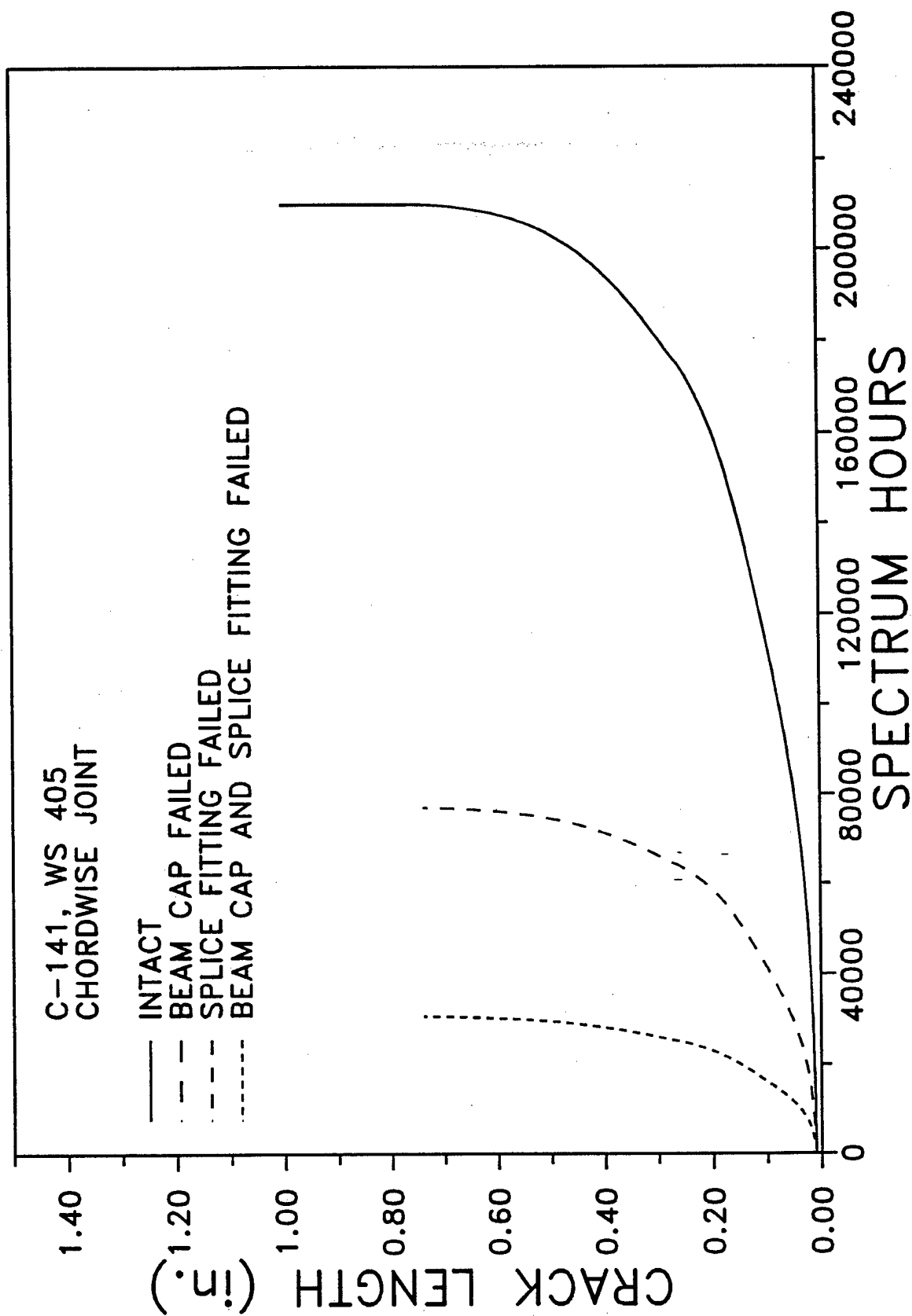


Figure 3 a Versus T - Chordwise Joint.

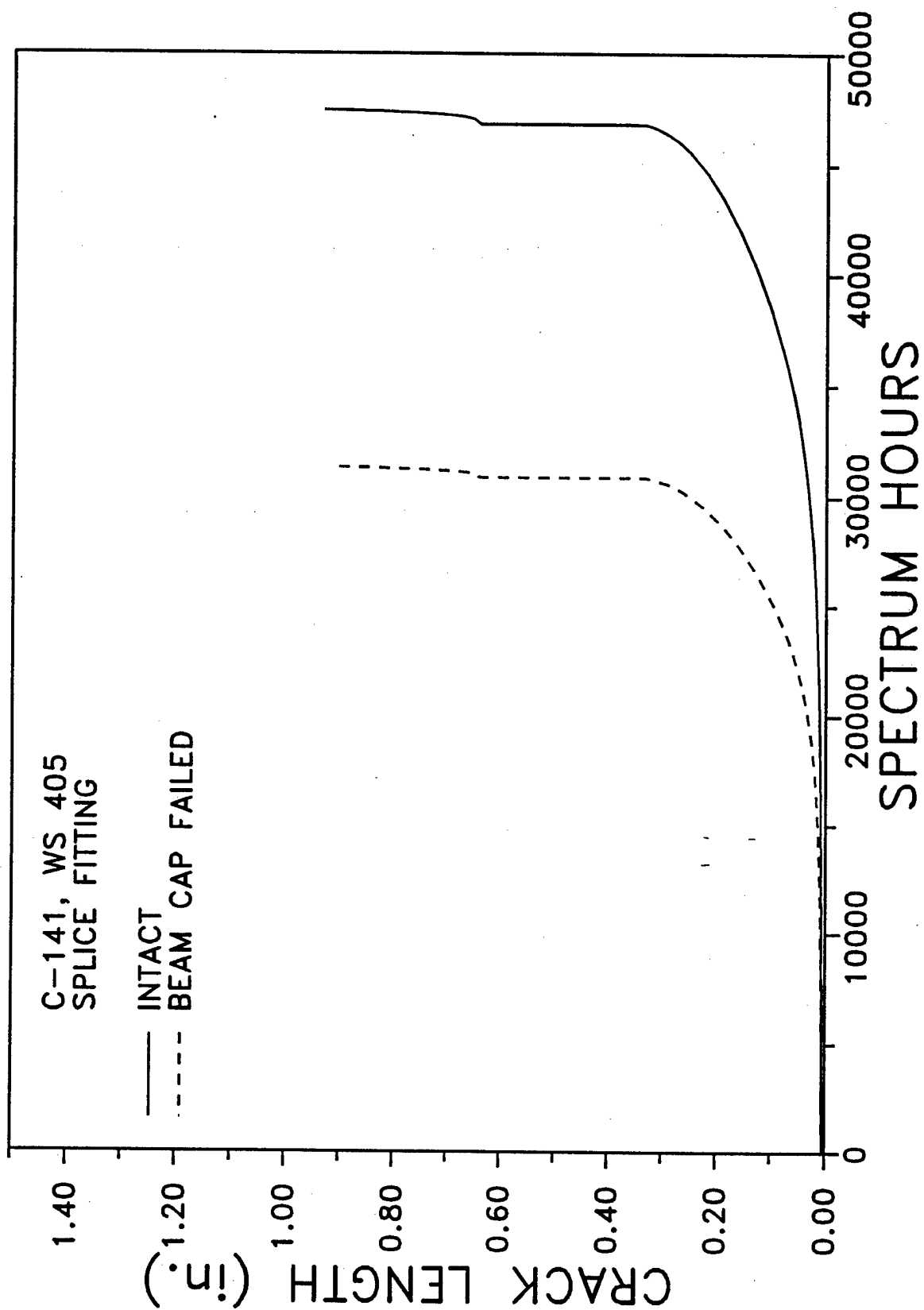


Figure 4 a Versus T - Splice Fitting.

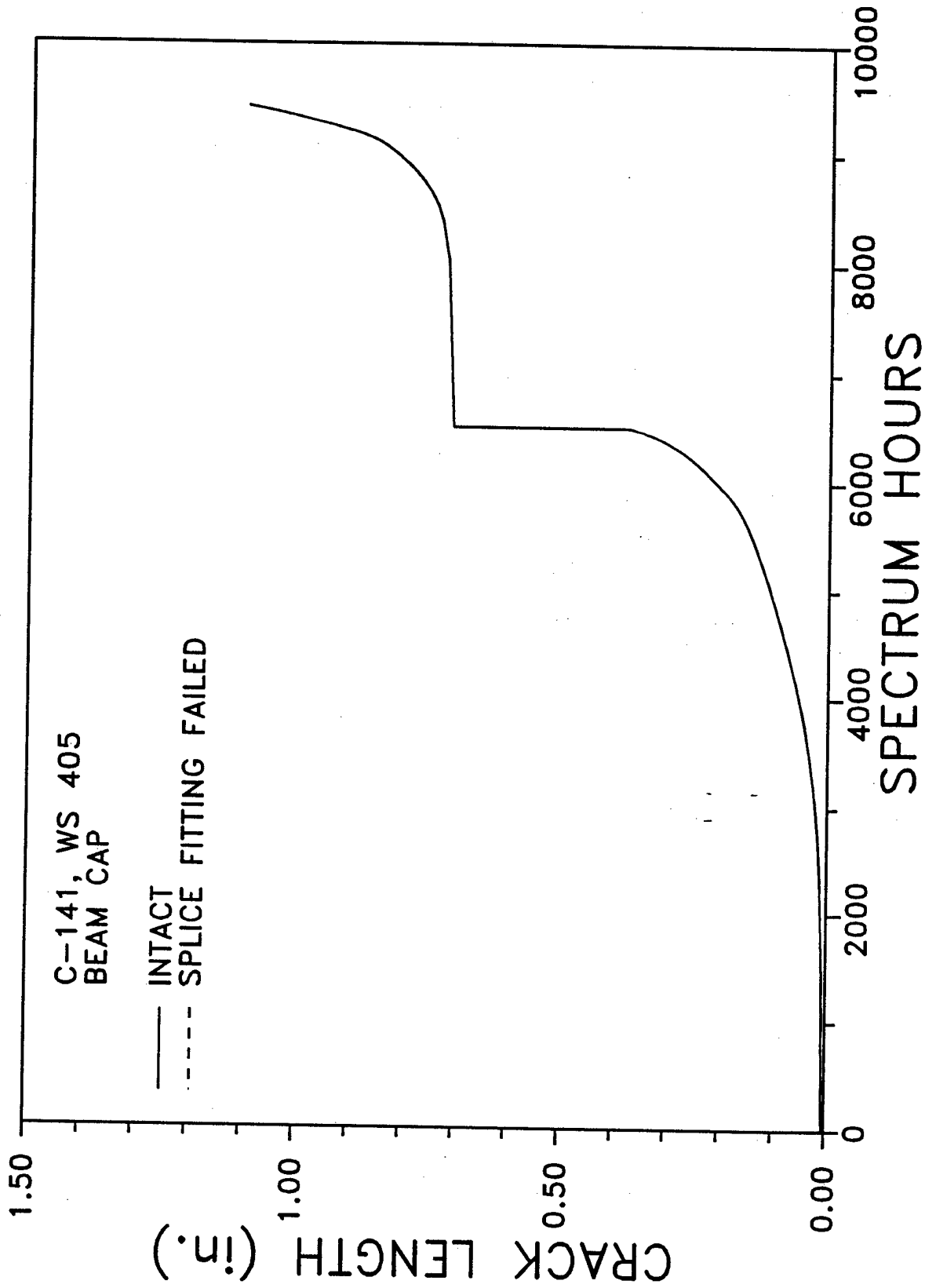


Figure 5 a Versus T - Beam Cap.



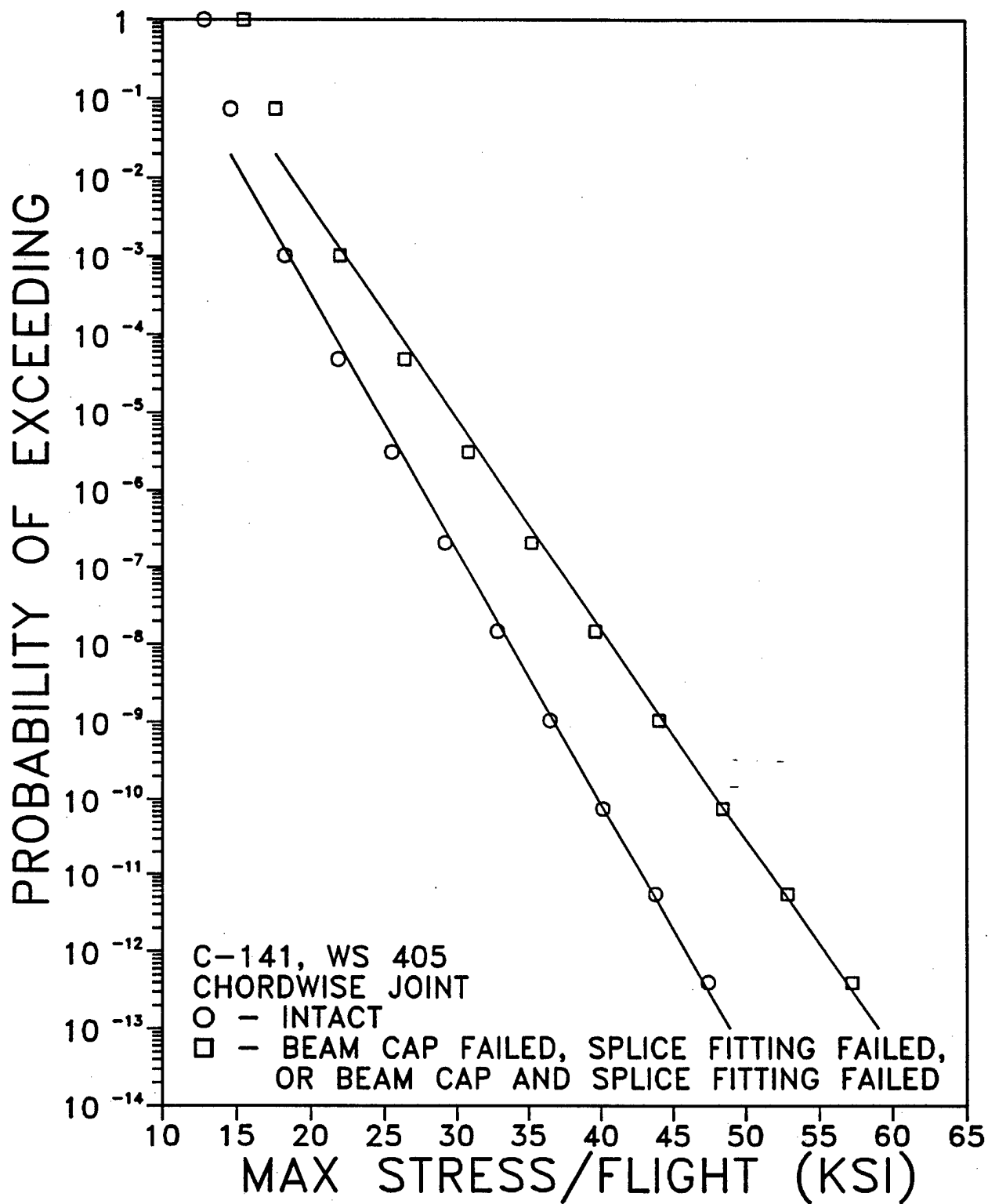


Figure 6 Distribution of Max Stress/Flight - Chordwise Joint.

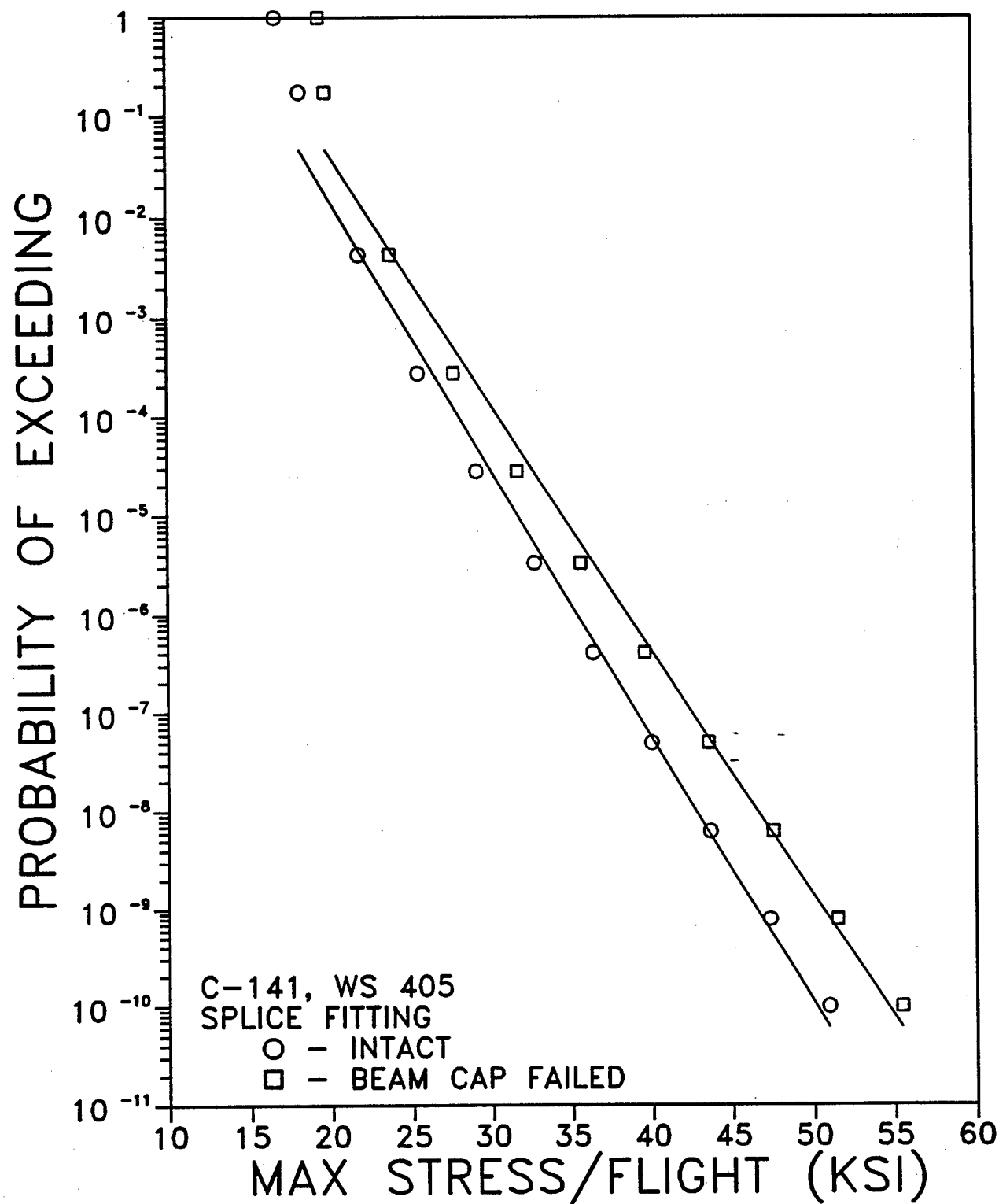


Figure 7 Distribution of Max Stress/Flight - Splice Fitting.

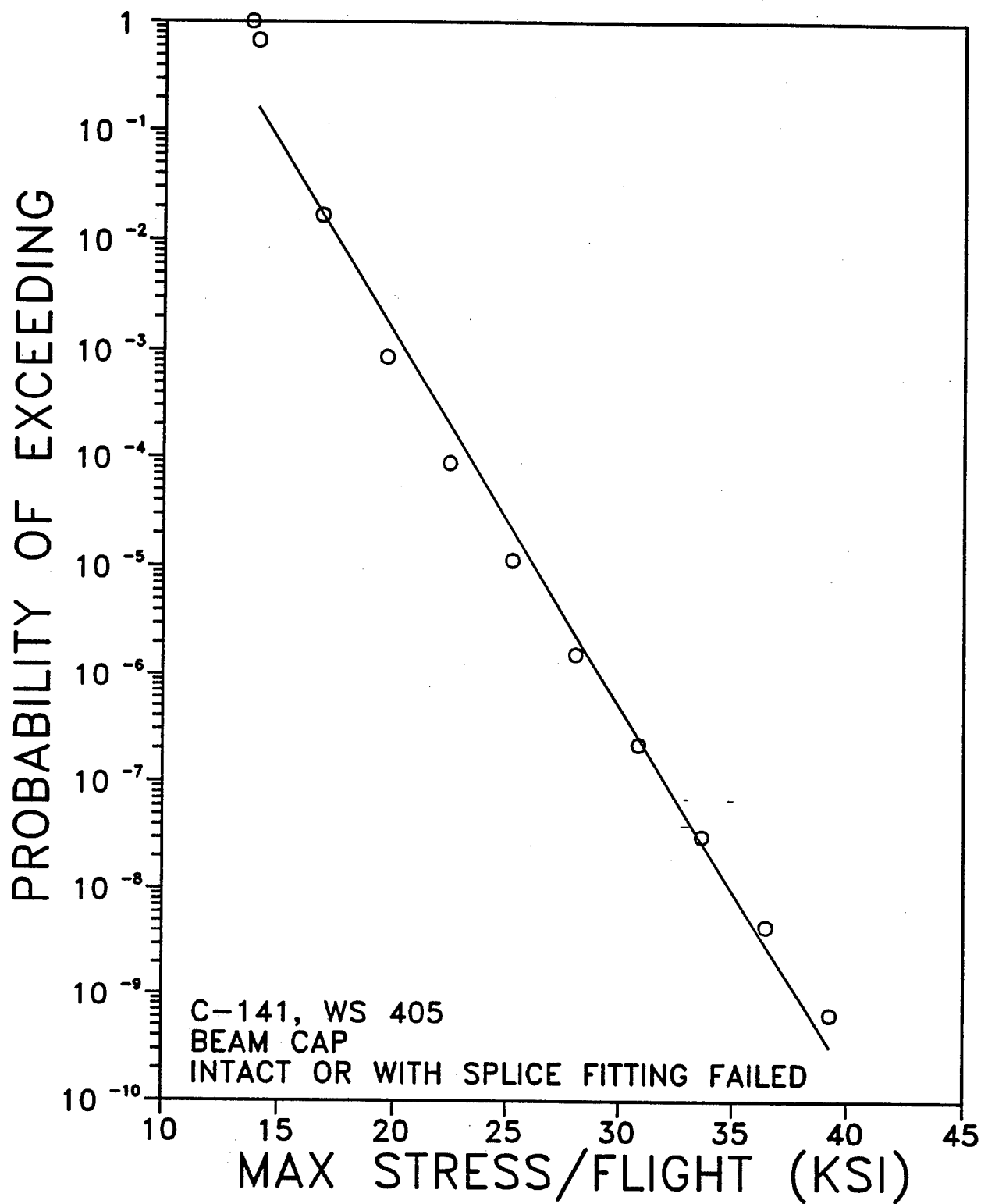


Figure 8 Distribution of Max Stress/Flight - Beam Cap.

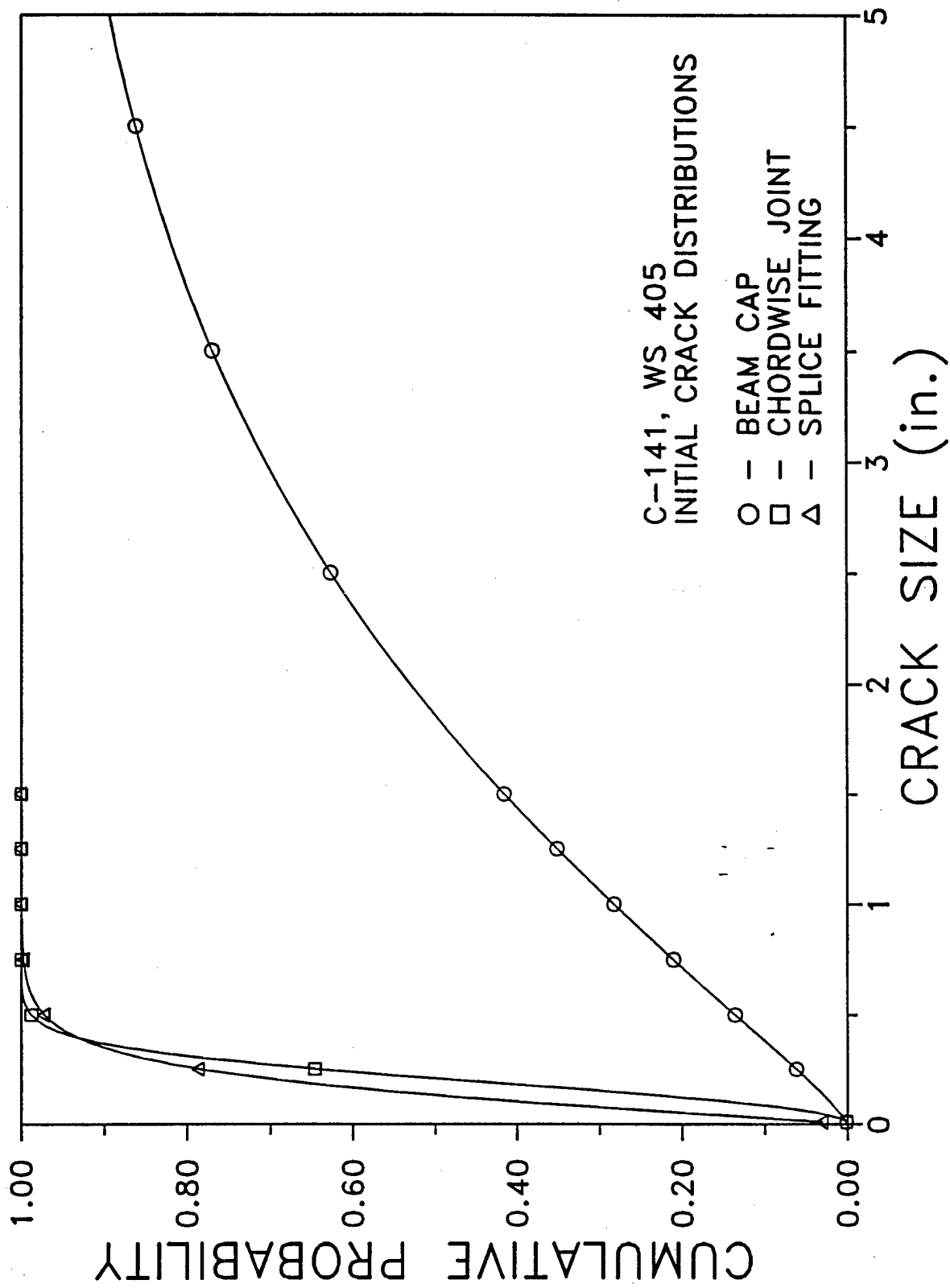


Figure 9 Initial Crack Size Distributions at 31,000 Hours.

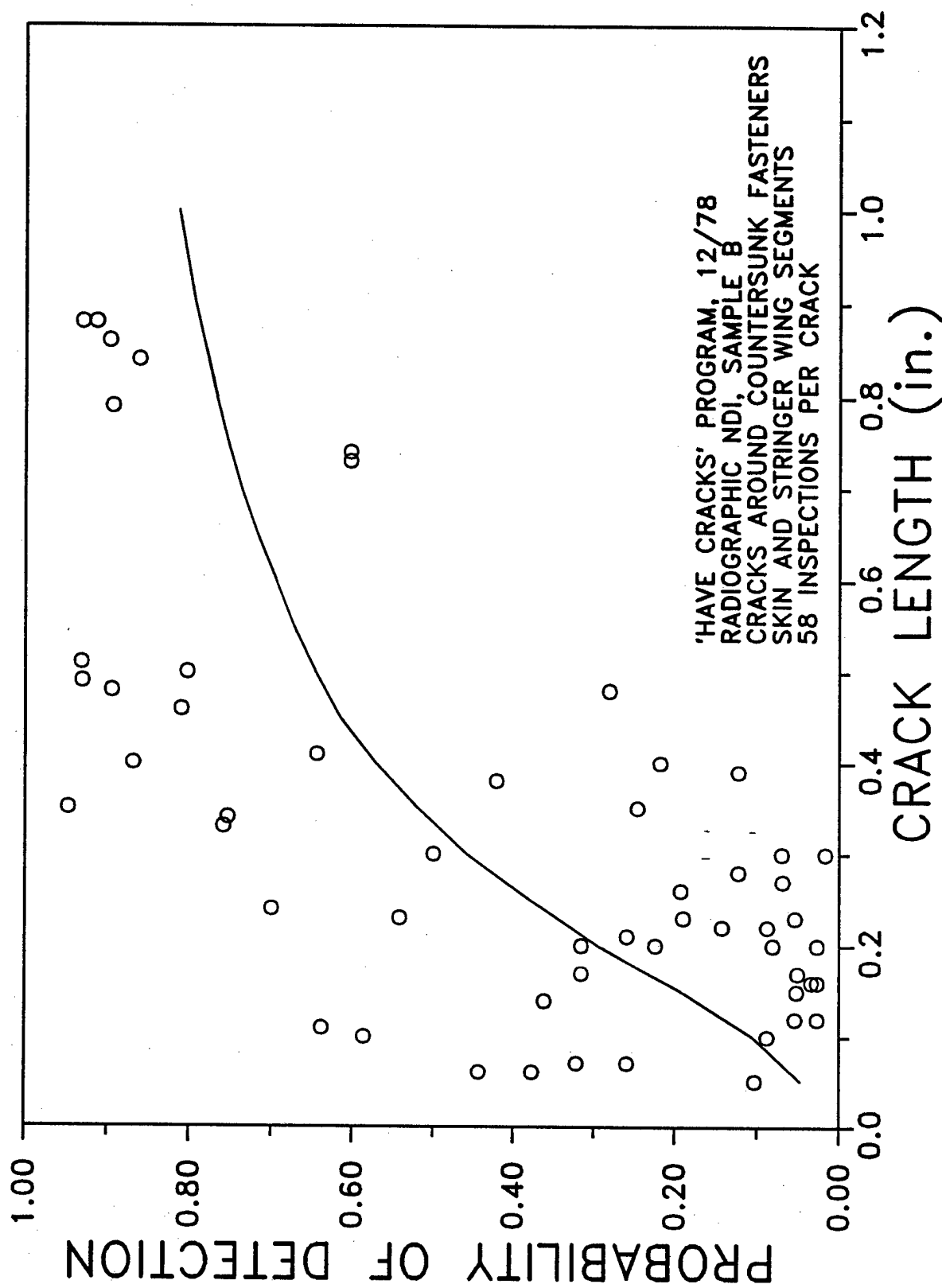


Figure 10 POD for X-Ray Inspections - 'Have Cracks' Data.

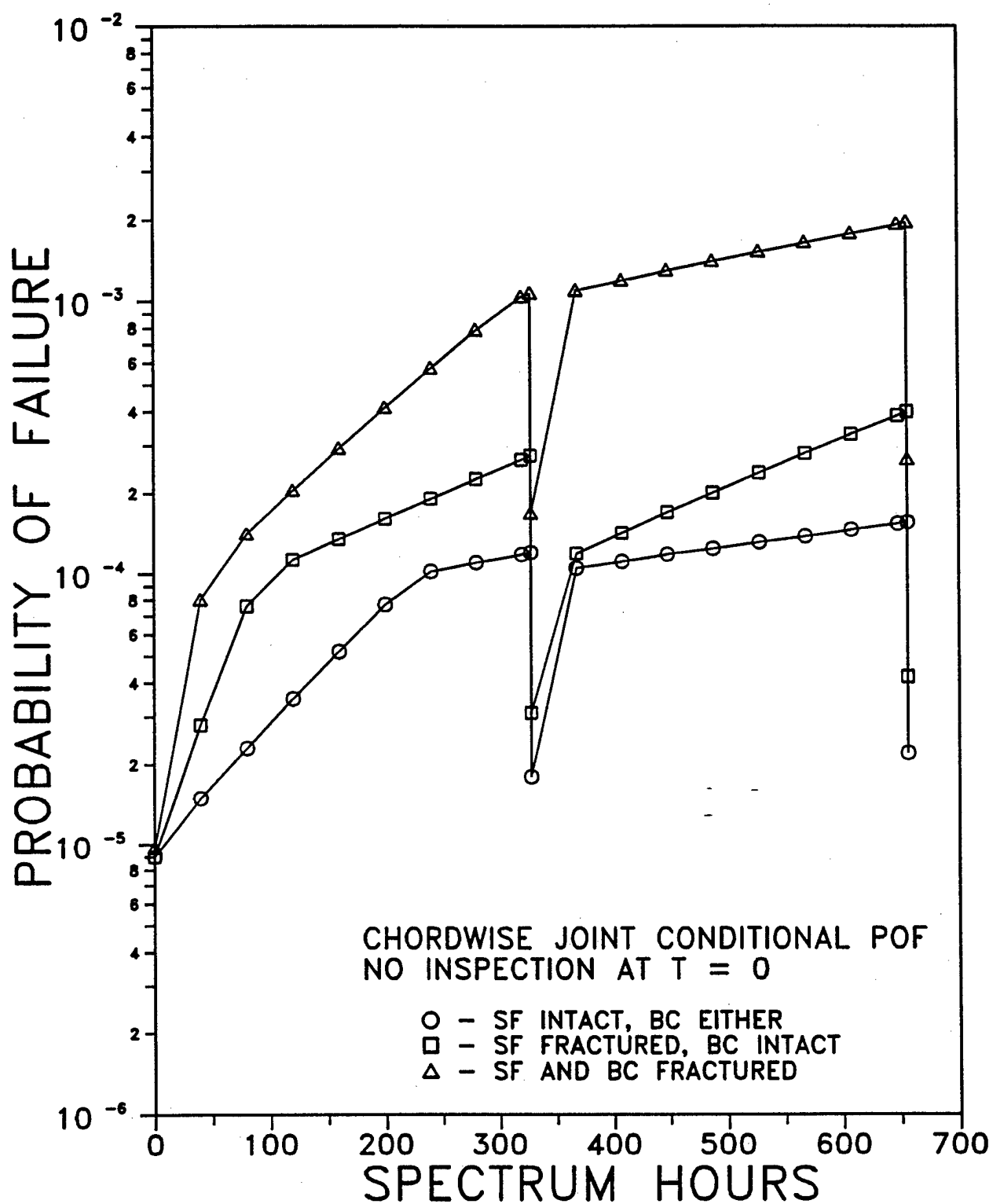


Figure 11 Conditional Failure Probabilities of Chordwise Joint - No Initial Inspection/Repair.

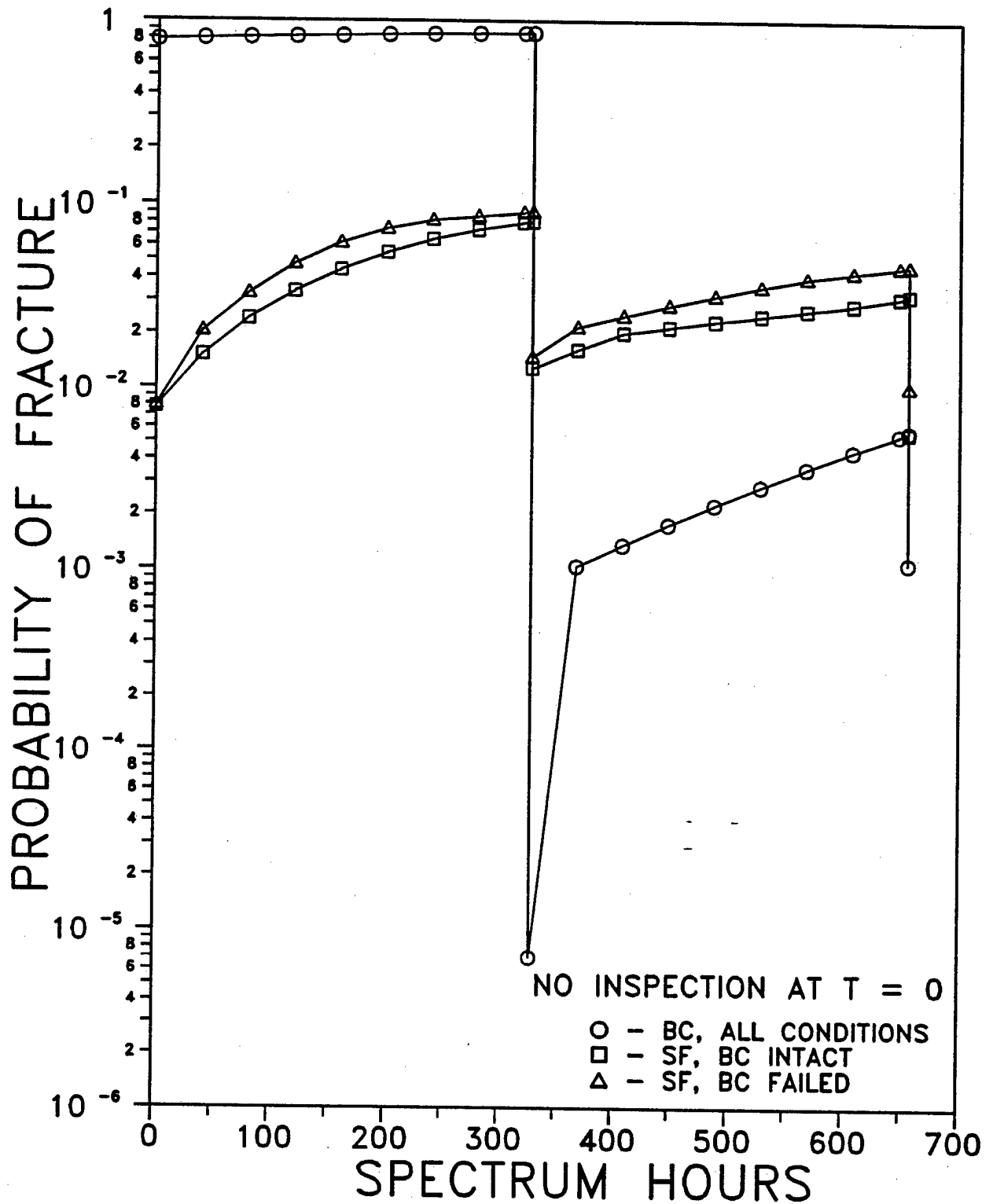


Figure 12 Failure Probabilities of Splice Fitting and Beam Cap - No Initial Inspection/Repair.

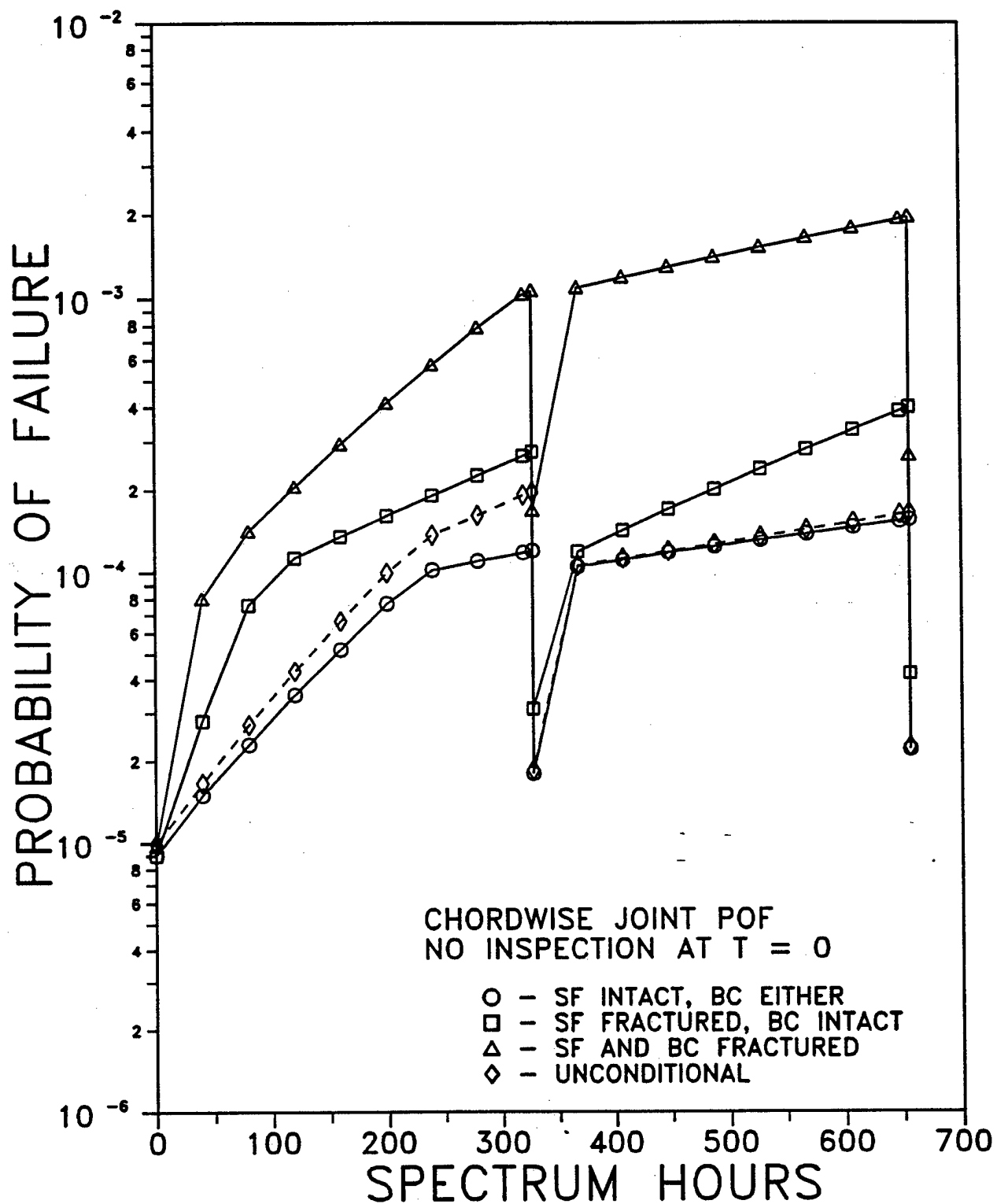


Figure 13 Unconditional Probability of Failure of Chordwise Joint - No Initial Inspection/Repair.



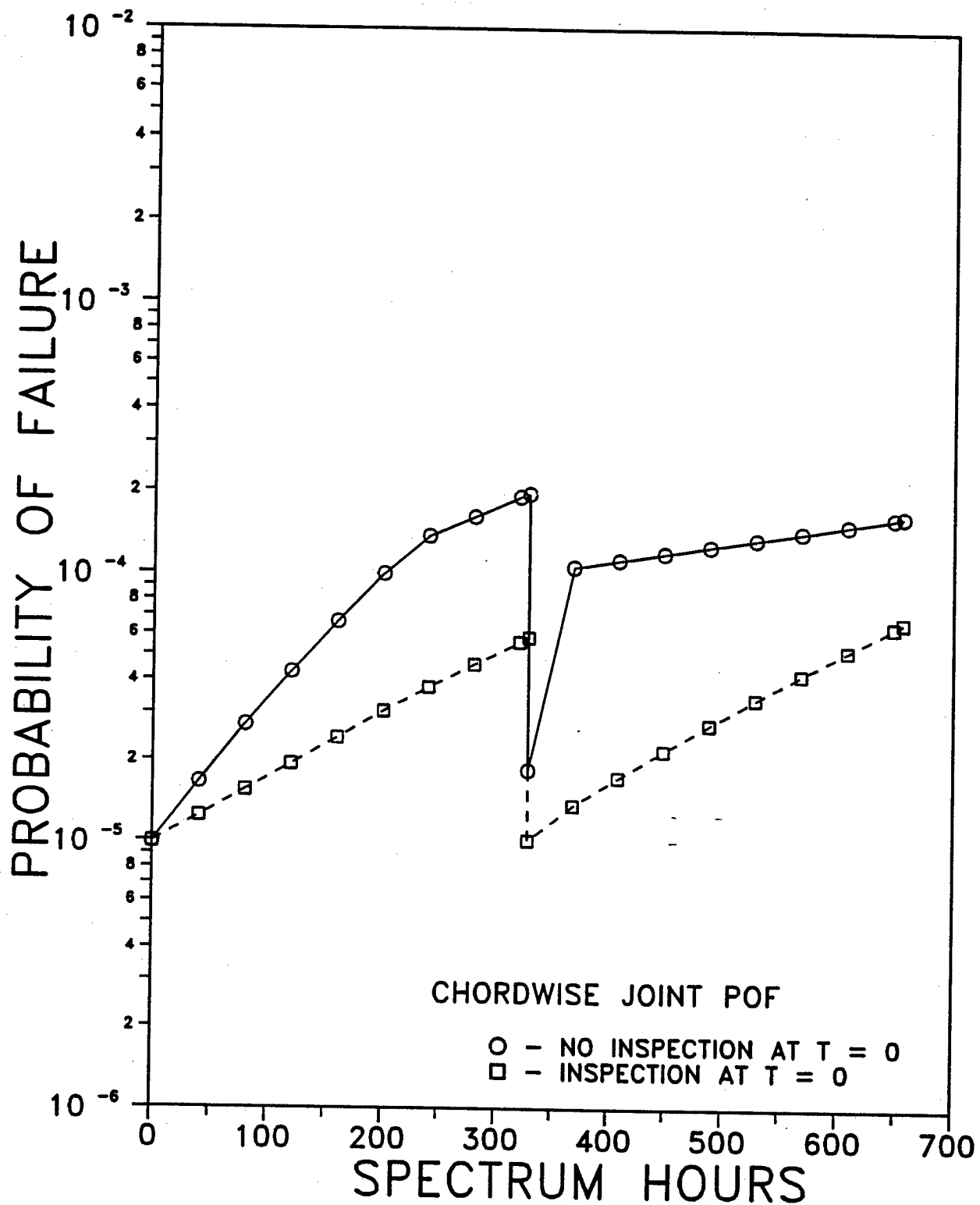


Figure 14 Unconditional Probability of Failure of Chordwise Joint - With and Without Initial Inspection/Repair.

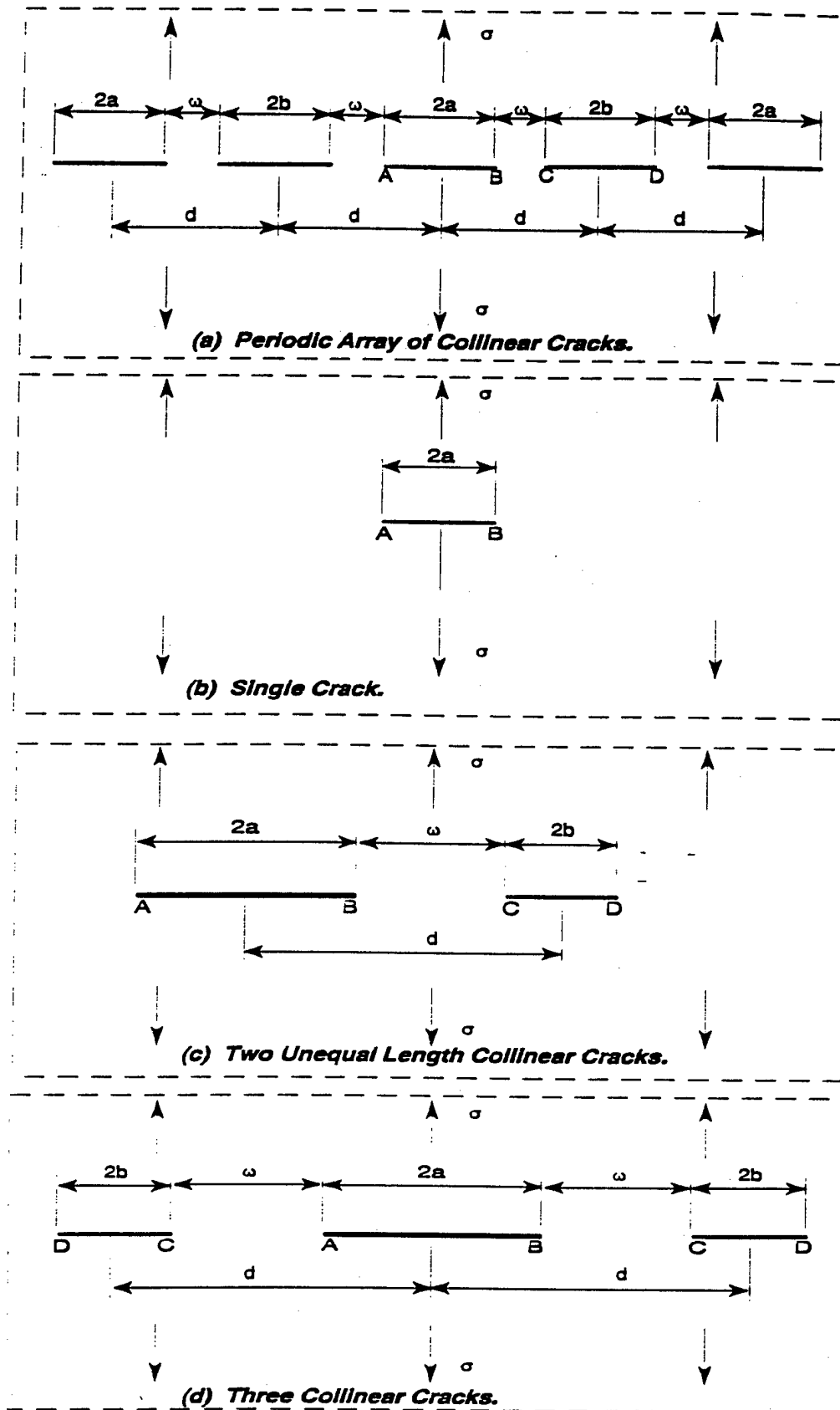


Figure 15 Crack Configurations

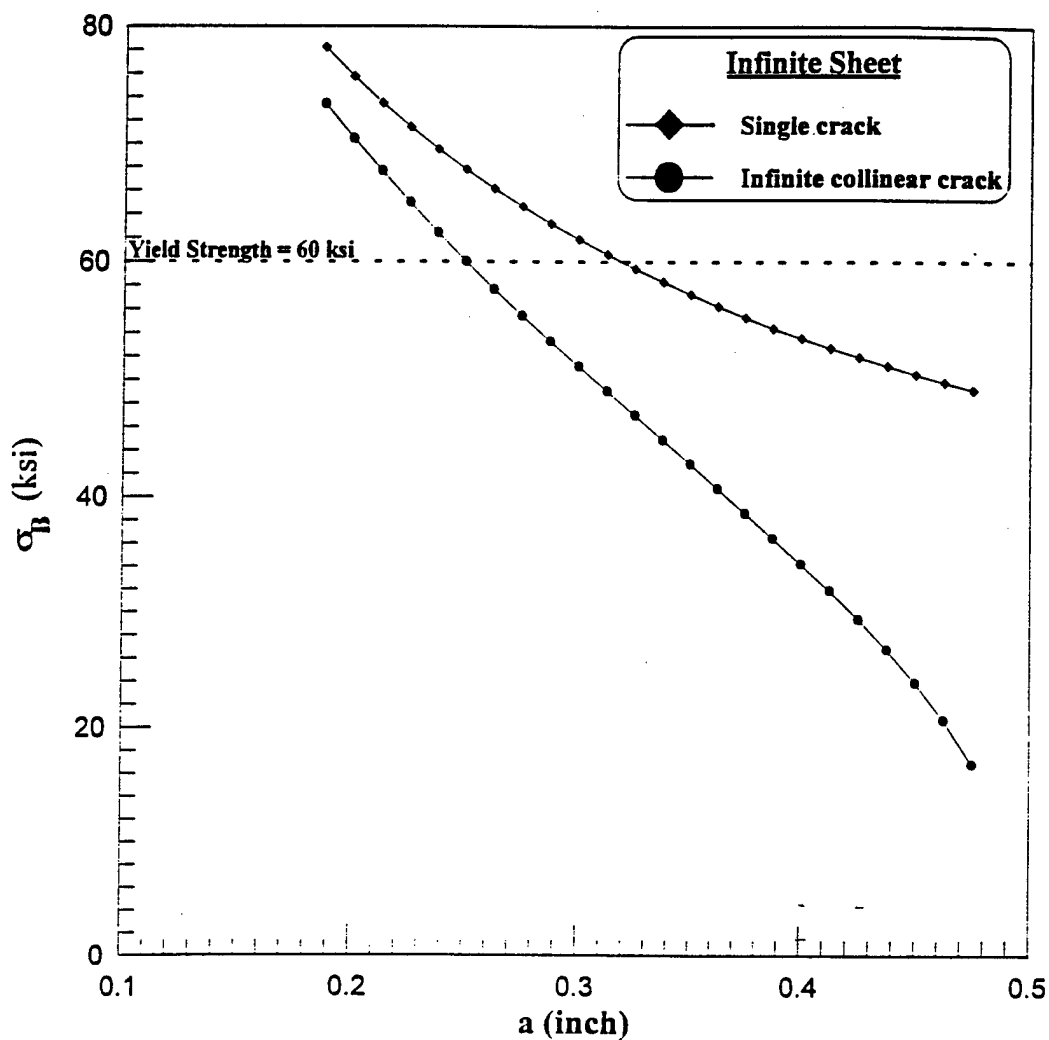


Figure 16 Comparison of Residual Strength Levels between Infinite Collinear Cracks and Single Crack in an Infinite Sheet Based on Critical Stress Intensity Factor Criterion.

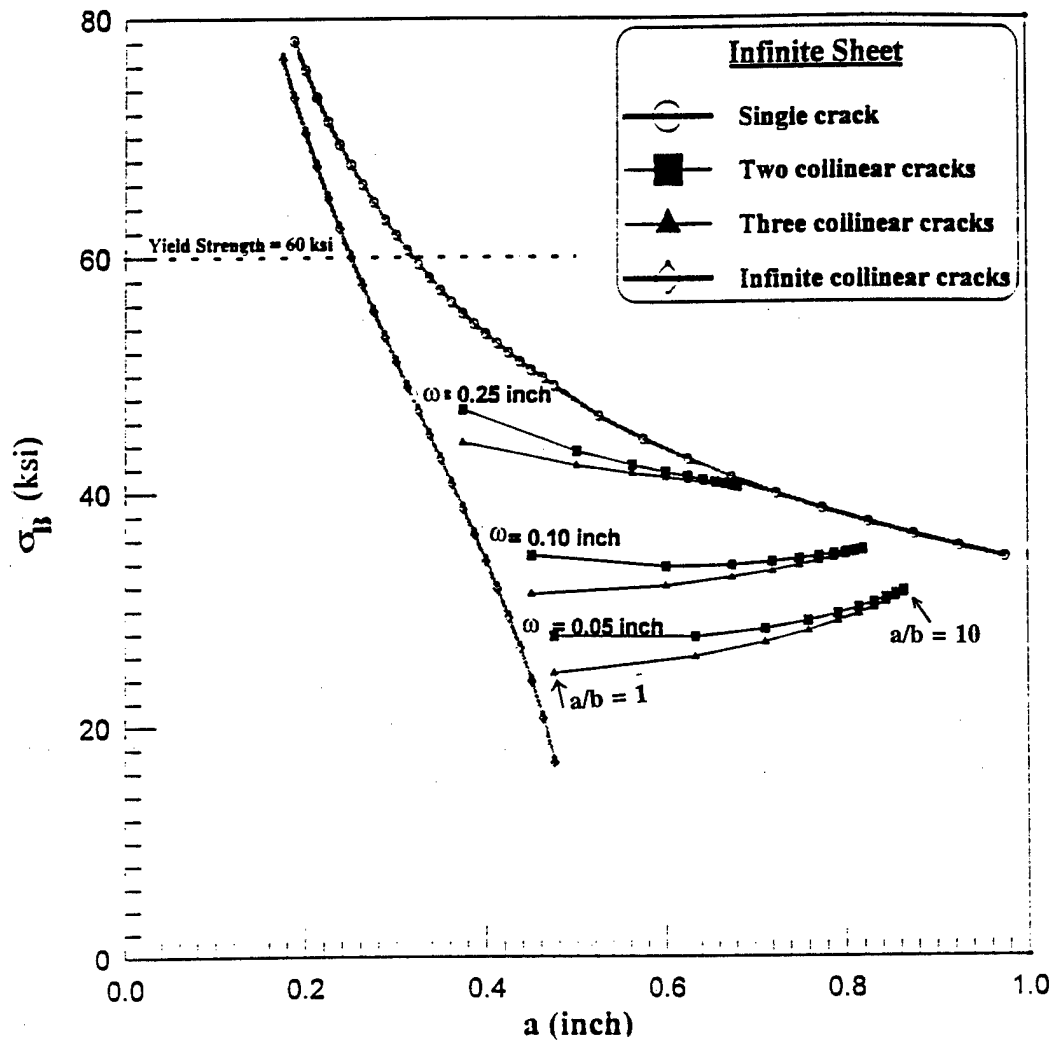


Figure 17 Comparison of Residual Strength Levels among (a) Single Crack, (b) Two Collinear Cracks, (c) Three Collinear Cracks and (d) Infinite Collinear Cracks, in an Infinite Sheet Based on Critical Stress Intensity Factor Criterion. Note:  $d = \text{constant}$  (1.0 inch)

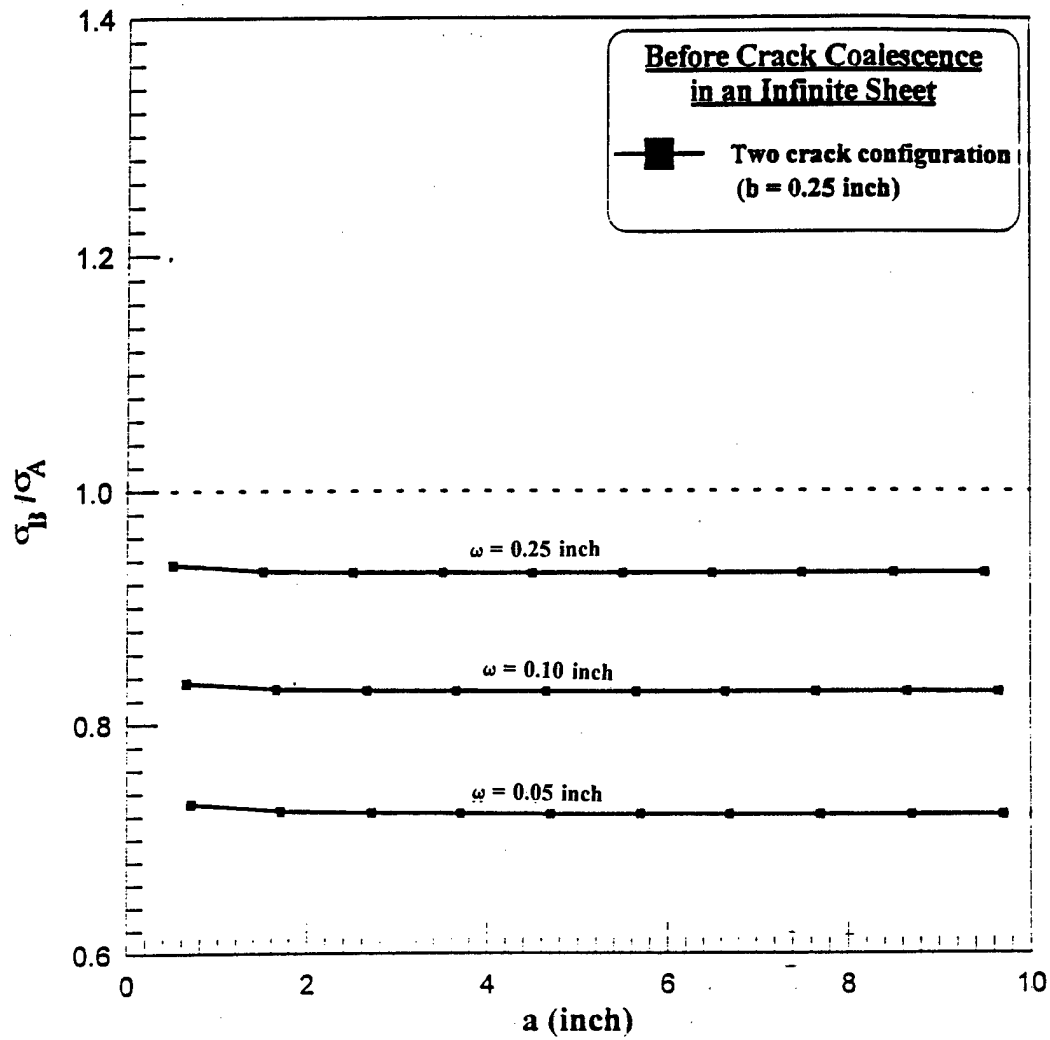


Figure 18 Ratio of Strength Levels for Extending Crack Tips B and A before Coalescence in Two Collinear Crack Configuration in an Infinite Sheet.

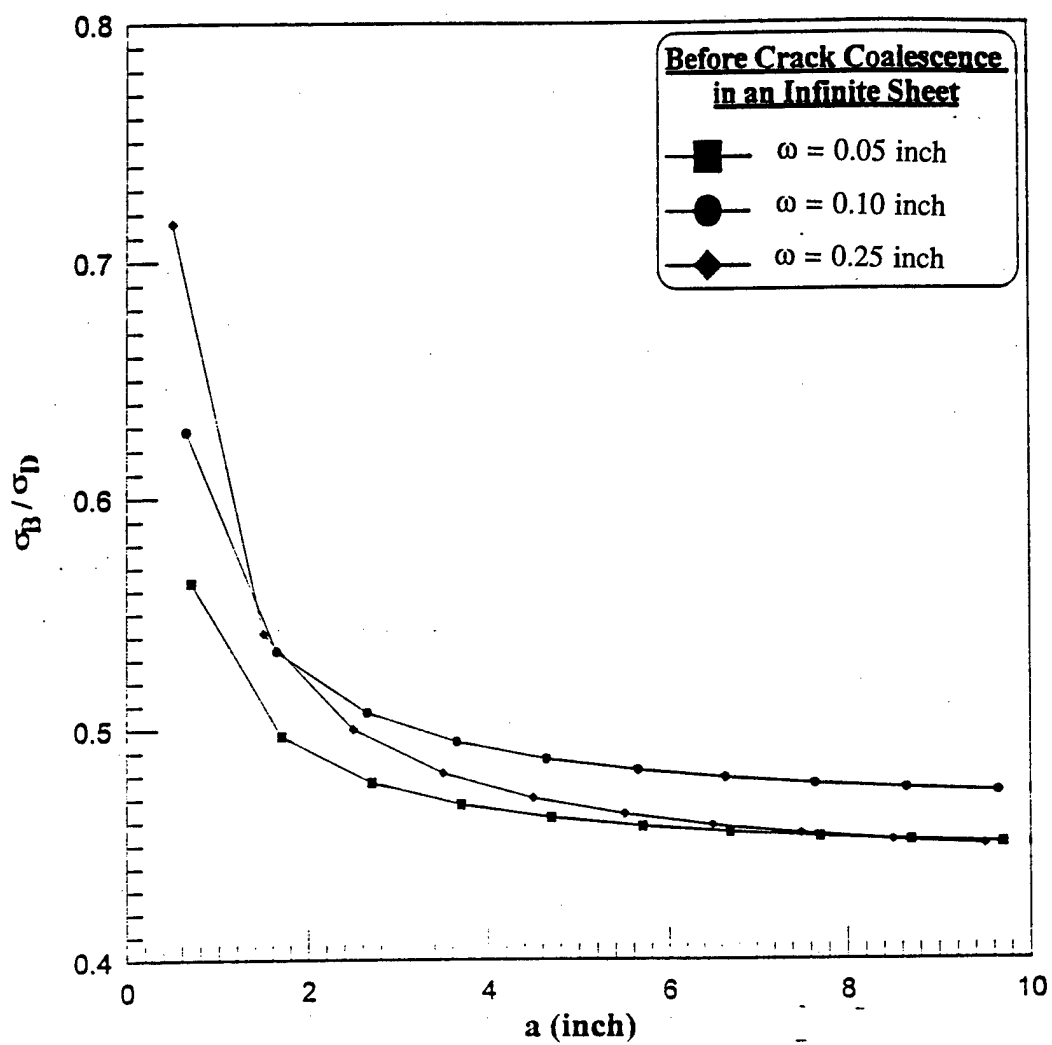


Figure 19 Ratio of Strength Levels for Extending Crack Tips B and D before Coalescence in Two Collinear Crack Configuration in an Infinite Sheet. Note:  $b = 0.25$  inch.

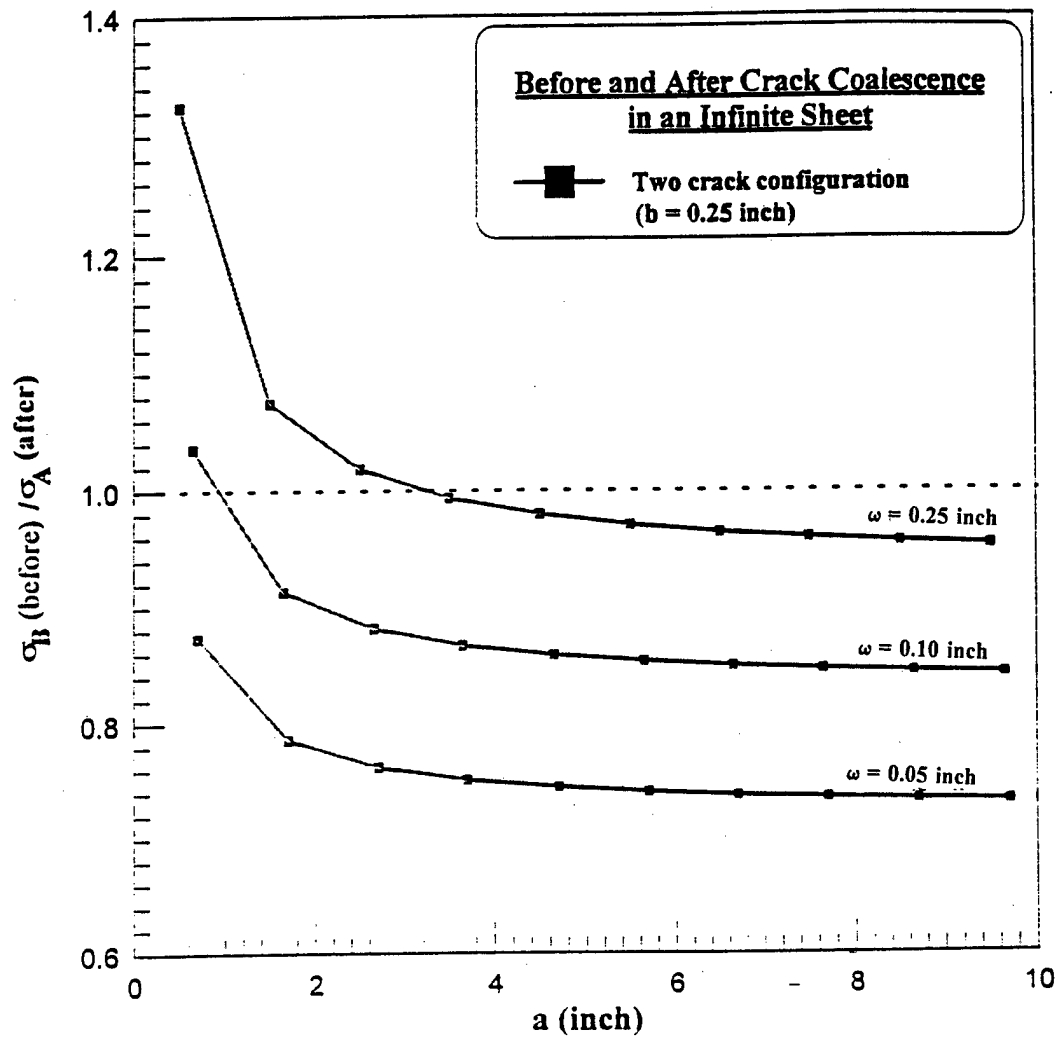


Figure 20 Effect of Largest Crack Size  $a$  on Coalescence Strength at Crack Tip B in Two Collinear Crack Configuration in an Infinite Sheet.

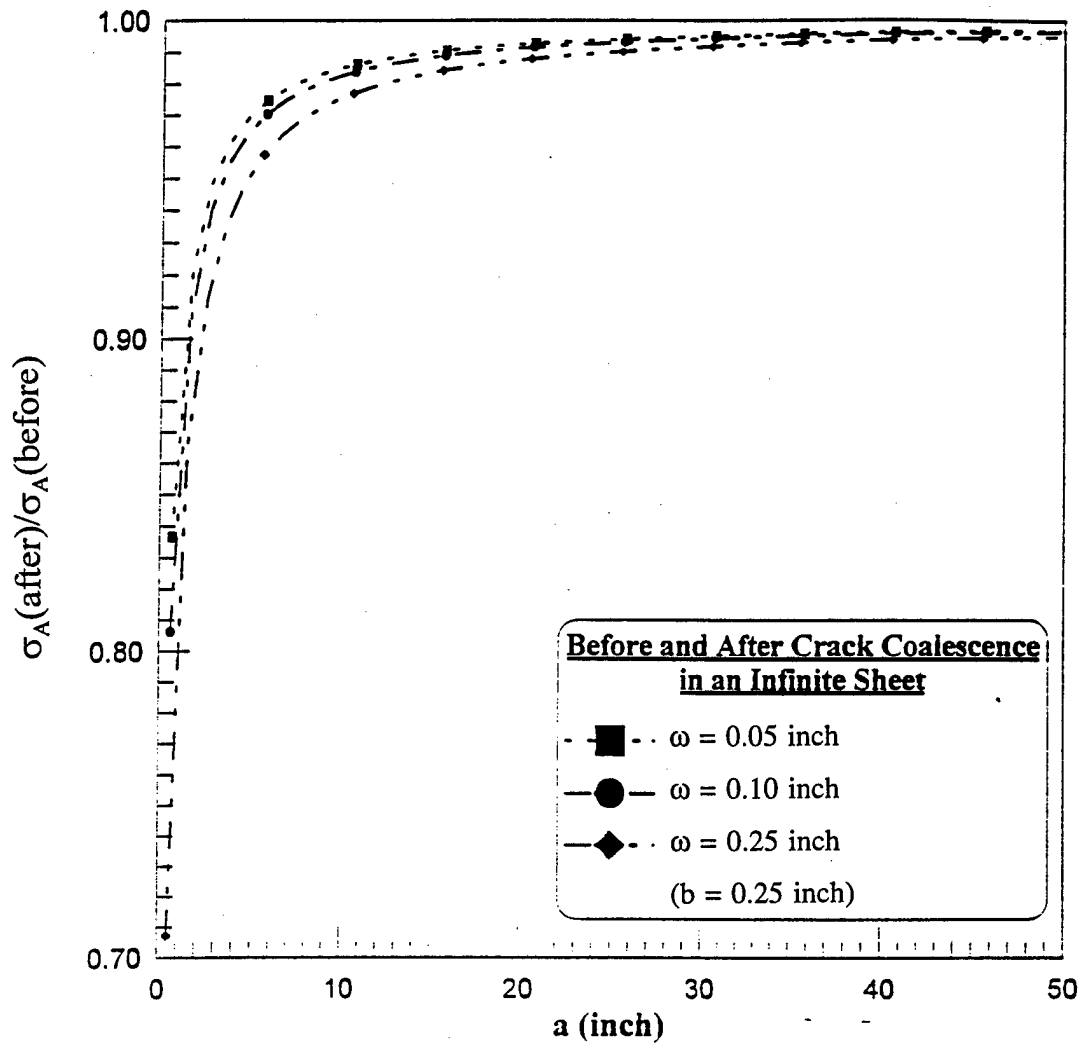


Figure 21 Effect of the Largest Crack Size  $a$  on Residual Strength Ratio (after/before) at Crack Tip A in Two Collinear Crack Configuration in an Infinite Sheet.



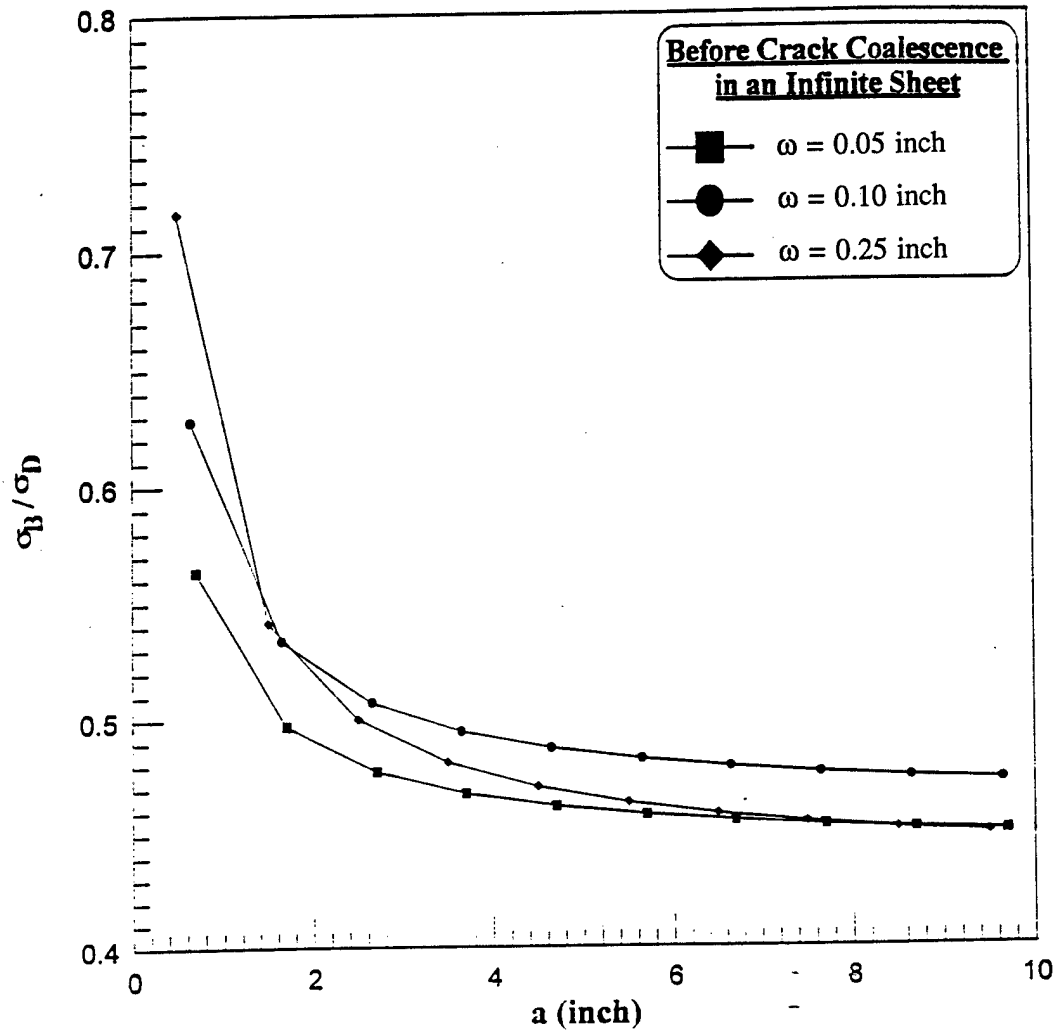


Figure 22 Ratio of Strength Levels for Extending Crack Tips B and D before Coalescence in Three Collinear Crack Configuration in an Infinite Sheet. Note:  $b = 0.25$  inch.

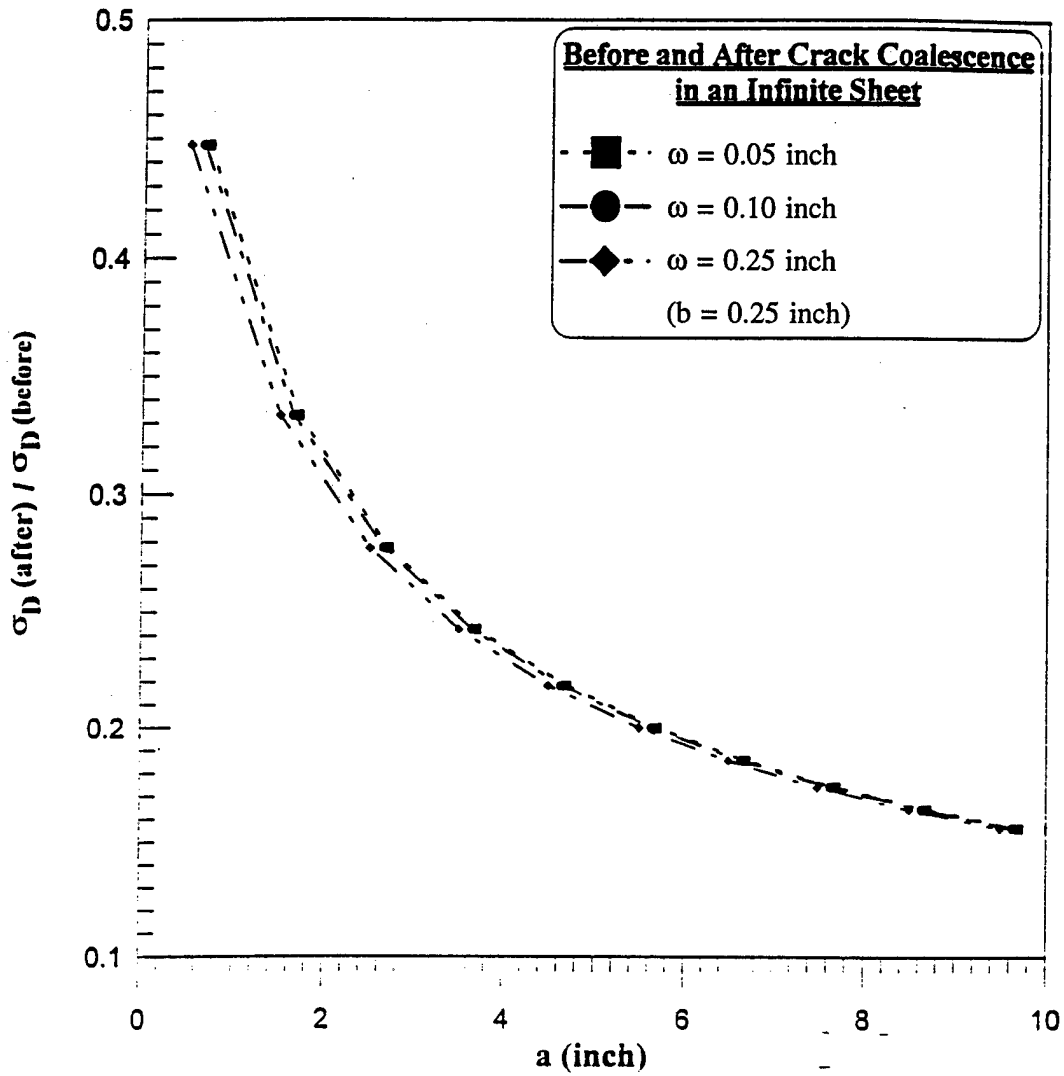


Figure 23 Effect of the largest Crack Size  $a$  on Residual Strength Ratio (after/before) at Crack Tip D in three Collinear Crack Configuration in an Infinite Sheet.

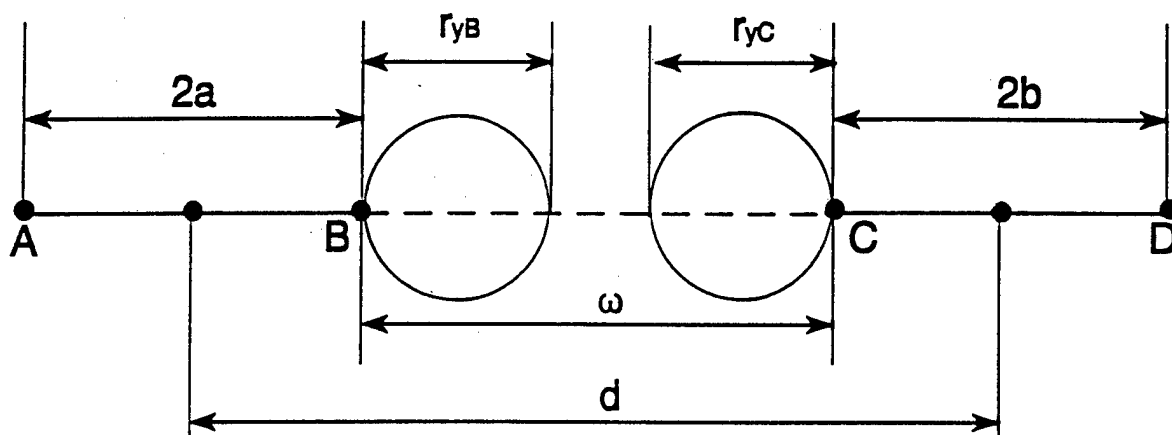


Figure 24 Swift Plastic Zone Interaction Model [22].

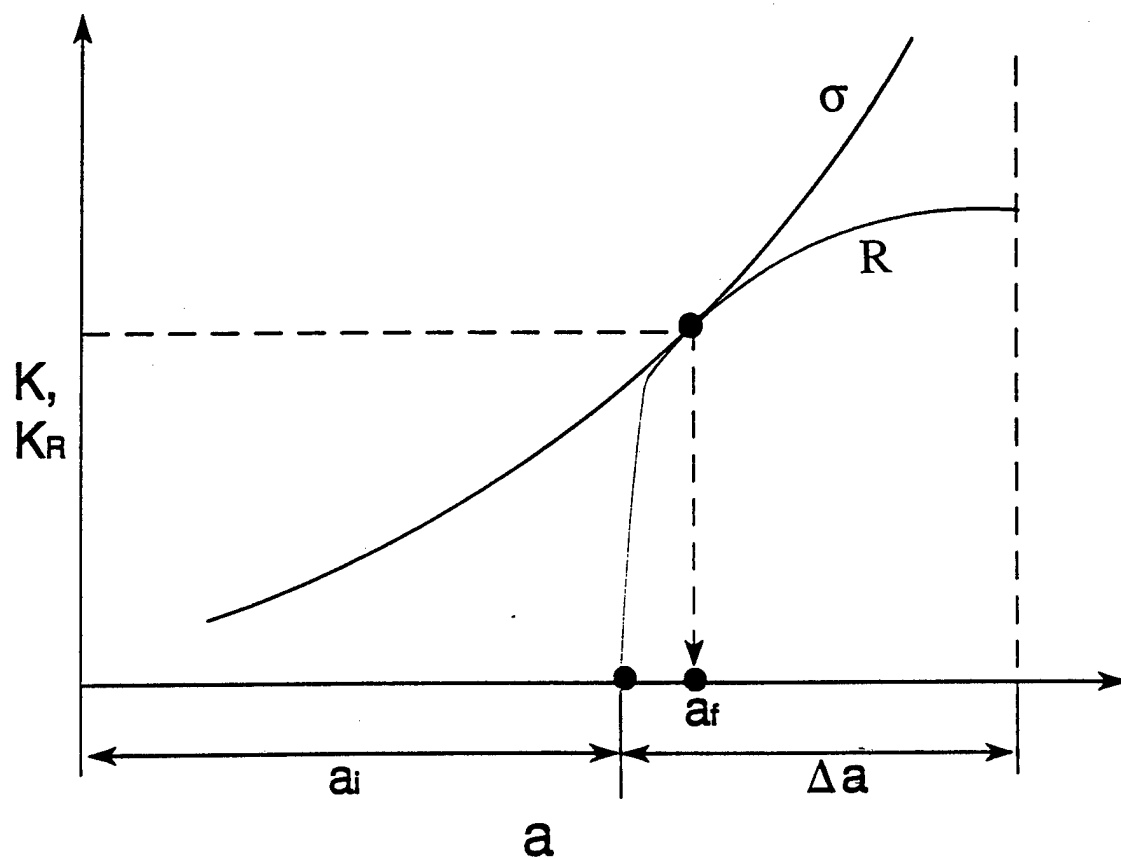


Figure 25 K-R Curve [21].

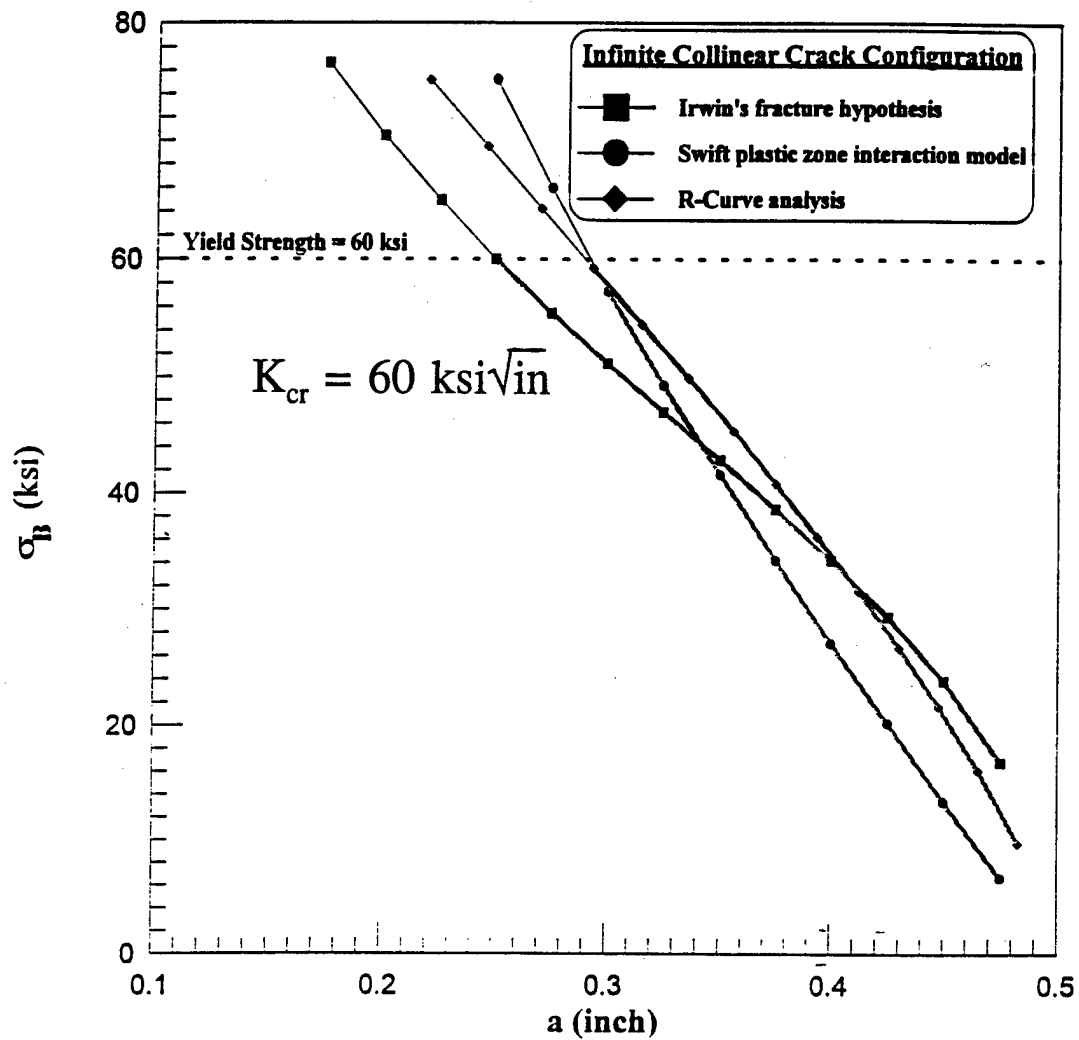


Figure 26 Effect of Fracture Criteria on the Residual Strength Level in an Infinite Collinear Cracks Configuration.

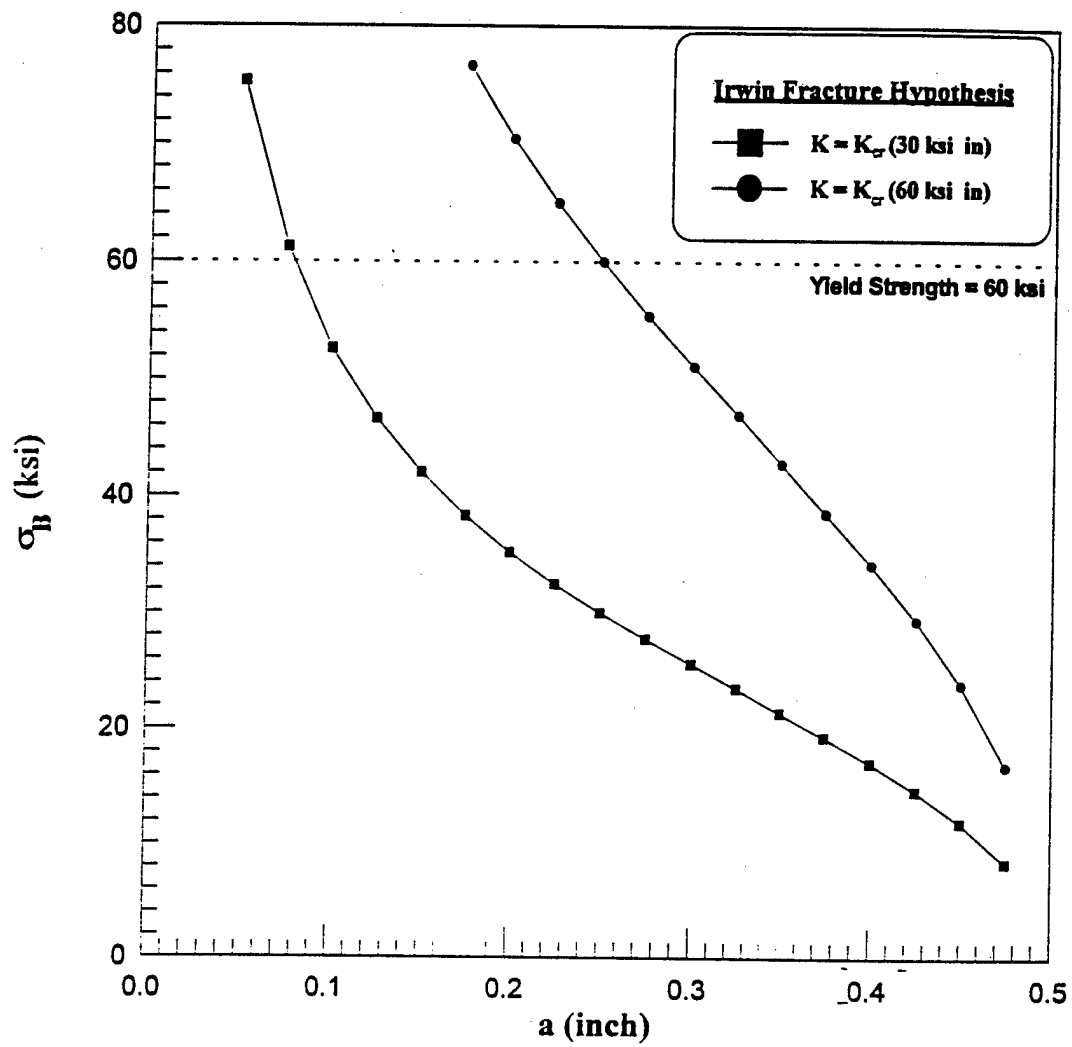


Figure 27 Effect of Fracture Toughness Level on Residual Strength Level in an Infinite Collinear Cracks Configuration.

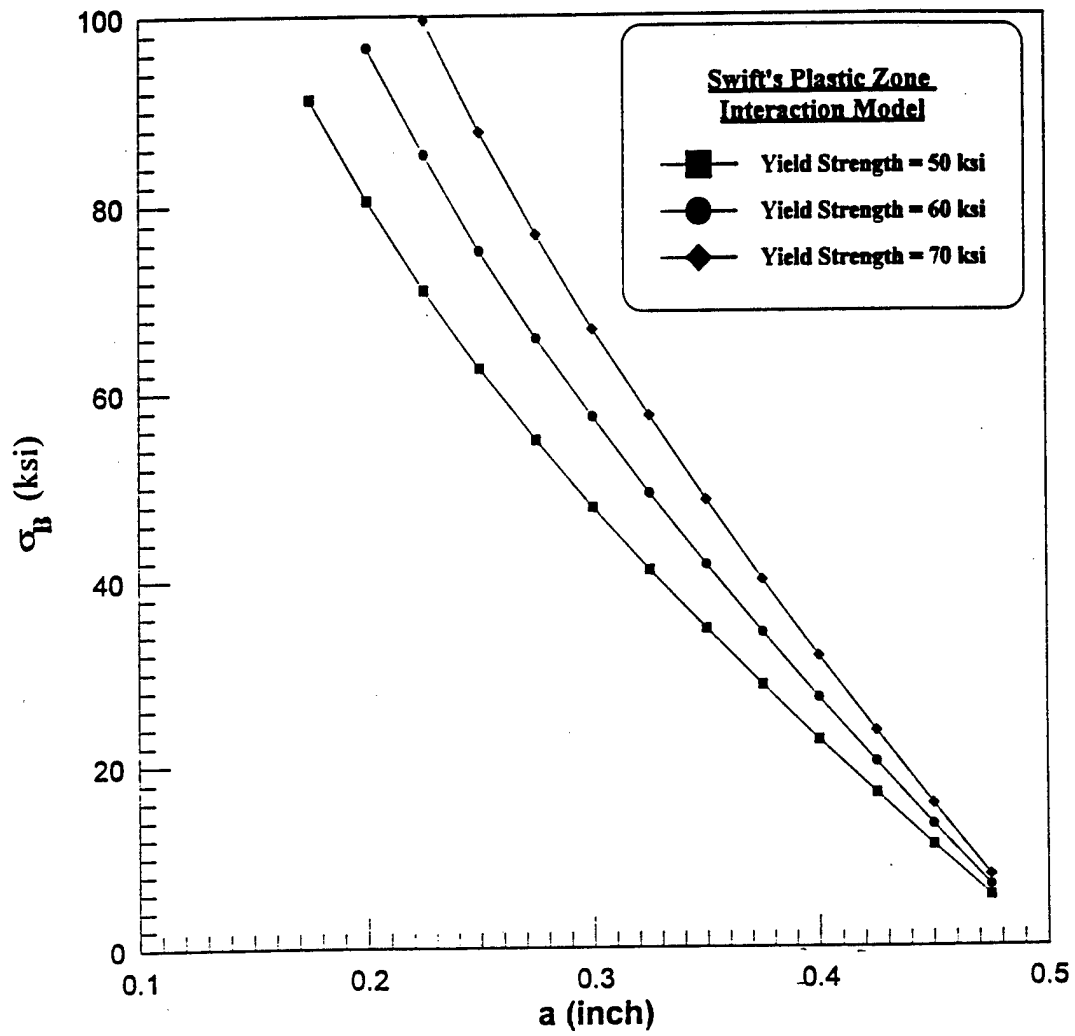


Figure 28 Effect of Yield Strength Level on Residual Strength Level in an Infinite Collinear Cracks Configuration.

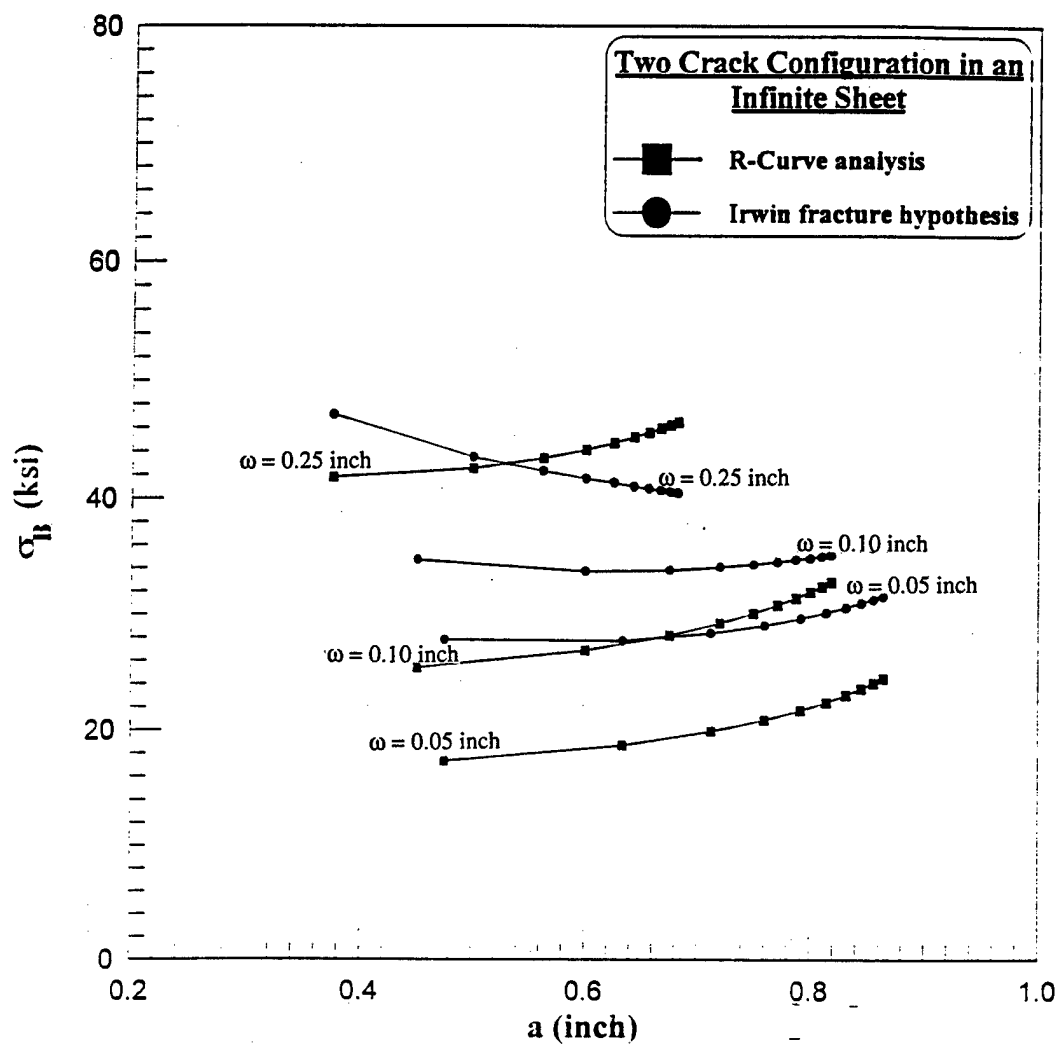


Figure 29 Comparison between R-Curve and Stress Intensity Factor Criteria to Identify the Lower Bound for the Residual Strength Level in the Two Collinear Crack Configuration.



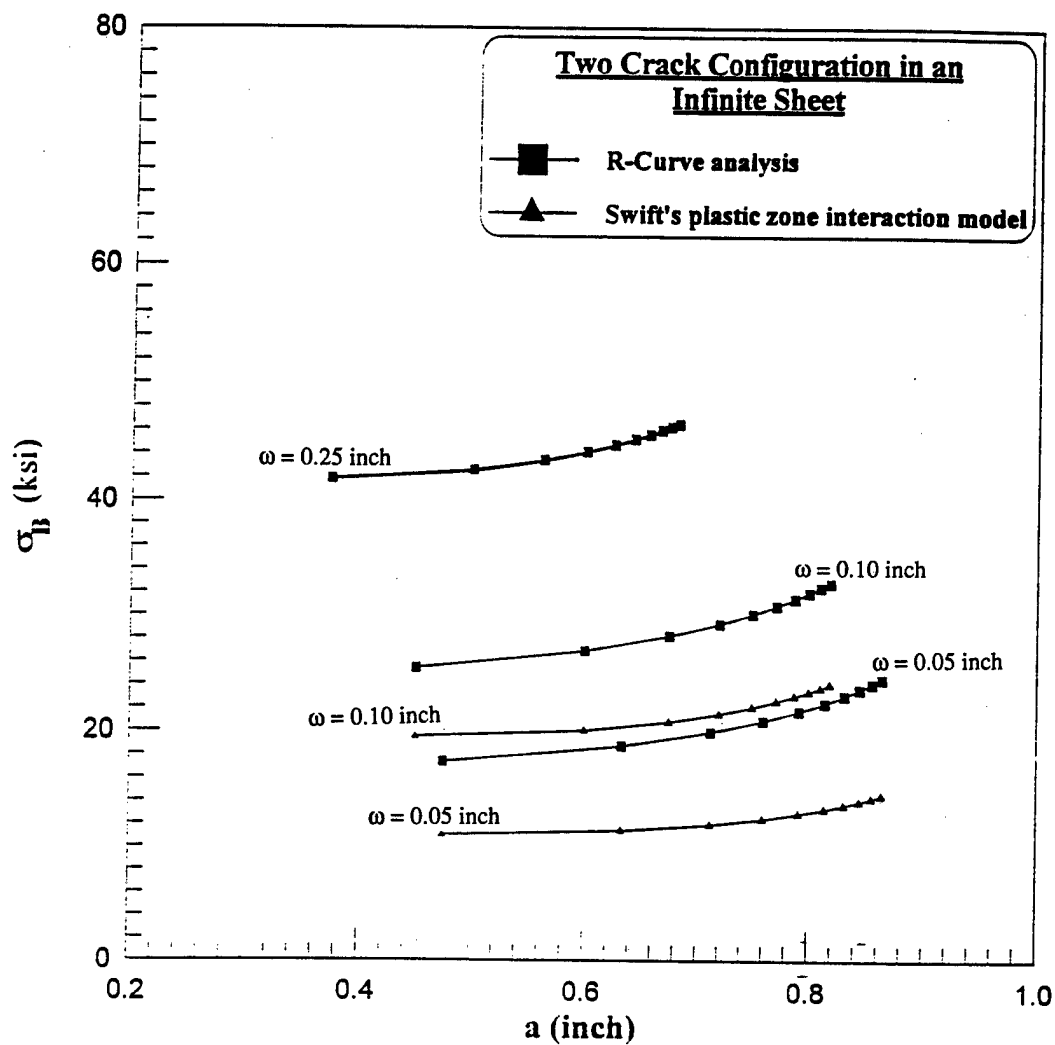


Figure 30 Comparison between R-Curve and Swift Plastic Zone Criteria to Identify the Lower Bound for the Residual Strength Level in Two Collinear Crack Configuration.